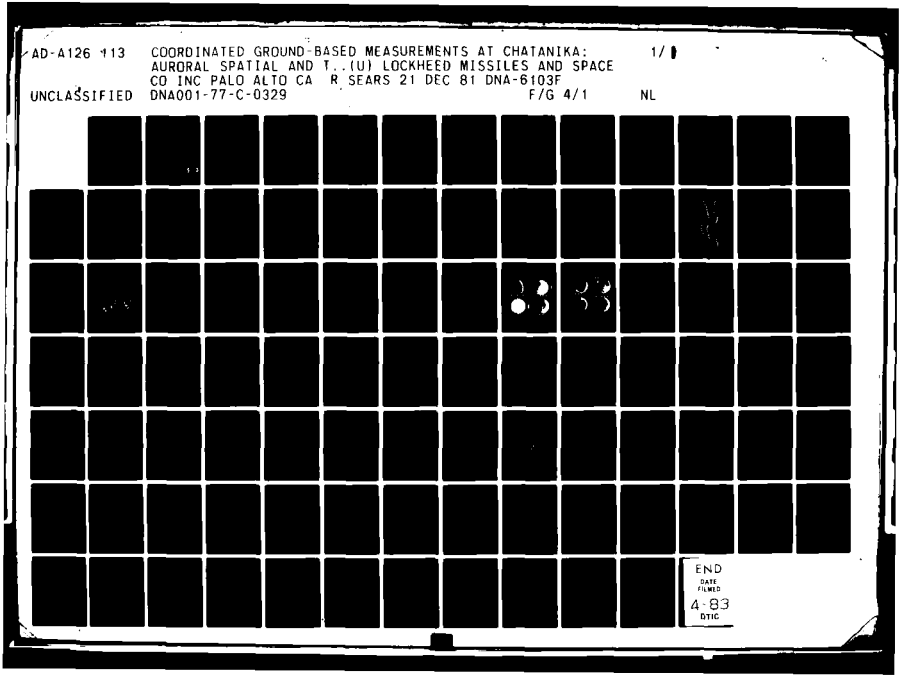
AD-A126 113 COORDINATED GROUND-BASED MEASUREMENTS AT CHATANIKA: 1/
AURORAL SPATIAL AND T..(U) LOCKHEED MISSILES AND SPACE
CO INC PALO ALTO CA R SEARS 21 DEC 81 DNA-6103F
UNCLASSIFIED DNA001-77-C-0329 F/G 4/1 NL
END
DATE FILMED
4-83
DTIC

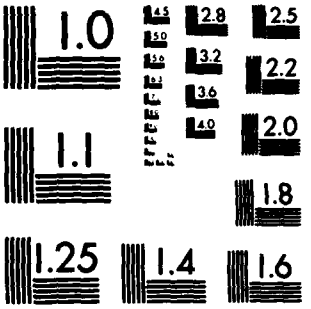

MICROCOPY RESOLUTION TEST CHART
NATIONAL BUREAU OF STANDARDS-1963-A

AD-E 301080

(12)

DNA 6103F

AD A126113

COORDINATED GROUND-BASED MEASUREMENTS AT CHATANIKA: AURORAL SPATIAL AND TEMPORAL STRUCTURE

Lockheed Missiles and Space Co., Inc.
3251 Hanover Street
Palo Alto, California 94304

21 December 1981

Final Report for Period 1 January 1979—21 December 1981

CONTRACT No. DNA 001-77-C-0329

APPROVED FOR PUBLIC RELEASE;
DISTRIBUTION UNLIMITED.

DTIC FILE COPY

THIS WORK WAS SPONSORED BY THE DEFENSE NUCLEAR AGENCY
UNDER RDT&E RMSS CODE B322078462 I25AAXHX63278 H2590D.

Prepared for
Director
DEFENSE NUCLEAR AGENCY
Washington, DC 20305

DTIC
ELECTE
MAR 2 4 1983
S D
B

83 03 025 032

Destroy this report when it is no longer needed. Do not return to sender.

PLEASE NOTIFY THE DEFENSE NUCLEAR AGENCY, ATTN: STTI, WASHINGTON, D.C. 20305, IF YOUR ADDRESS IS INCORRECT, IF YOU WISH TO BE DELETED FROM THE DISTRIBUTION LIST, OR IF THE ADDRESSEE IS NO LONGER EMPLOYED BY YOUR ORGANIZATION.

UNCLASSIFIED

SECURITY CLASSIFICATION OF THIS PAGE (When Data Entered)

REPORT DOCUMENTATION PAGE		READ INSTRUCTIONS BEFORE COMPLETING FORM
1. REPORT NUMBER 6103F	2. GOVT ACCESSION NO. AD-A126113	3. RECIPIENT'S CATALOG NUMBER
4. TITLE (and Subtitle) COORDINATED GROUND-BASED MEASUREMENTS AT CHATANIKA: AURORAL SPATIAL AND TEMPORAL STRUCTURE		5. TYPE OF REPORT & PERIOD COVERED Final Report for Period 1 Jan 79—21 Dec 81 6. PERFORMING ORG. REPORT NUMBER
7. AUTHOR(s) R. D. Sears		8. CONTRACT OR GRANT NUMBER(s) DNA 001-77-C-0329
9. PERFORMING ORGANIZATION NAME AND ADDRESS Lockheed Missiles and Space Co., Inc. 3251 Hanover Street Palo Alto, California 94304		10. PROGRAM ELEMENT, PROJECT, TASK AREA & WORK UNIT NUMBERS Subtask I25AAXHX632-78
11. CONTROLLING OFFICE NAME AND ADDRESS Director Defense Nuclear Agency Washington, D.C. 20305		12. REPORT DATE 21 December 1981 13. NUMBER OF PAGES 92
14. MONITORING AGENCY NAME & ADDRESS(if different from Controlling Office)		15. SECURITY CLASS. (of this report) UNCLASSIFIED 15a. DECLASSIFICATION/DOWNGRADING SCHEDULE N/A since UNCLASSIFIED

16. DISTRIBUTION STATEMENT (of this Report)

Approved for public release; distribution unlimited.

17. DISTRIBUTION STATEMENT (of the abstract entered in Block 20, if different from Report)

18. SUPPLEMENTARY NOTES

This work was sponsored by the Defense Nuclear Agency under RDT&E RMSS Code B322078462 I25AAXHX63278 H2590D.

19. KEY WORDS (Continue on reverse side if necessary and identify by block number)

Aurora	Structure	Atmospheric Radiance
Airglow	Temporal PSD	Electron Density
Spectrophotometry	Spatial PSD	Ionosphere

20. ABSTRACT (Continue on reverse side if necessary and identify by block number)

Spectrophotometric measurements of the auroral emission intensities in several wavelength regions were made at Chatanika Alaska during observing periods in 1978 through 1980. Specific experiments reported herein include: measurements of the temporal and spatial power spectral densities and associated statistical quantities for auroral emission irregularities which occurred during the development, intensification, and decay of a poleward expansion; characterization of the precipitating electron flux, total energy deposit and

DD FORM 1 JAN 73 1473 EDITION OF 1 NOV 65 IS OBSOLETE

UNCLASSIFIED

SECURITY CLASSIFICATION OF THIS PAGE (When Data Entered)

20. ABSTRACT (Continued)

mean energy parameter, and the response of the ionosphere during an intense pulsating aurora, and observation of the precipitating electron flux characteristics and the ionospheric response over a period of decaying precipitation intensity located at the poleward edge of the aurora oval. Both of the latter measurements were conducted as coordinated experiments with the Chatanika incoherent scatter radar.

The results of these experiments cover a range of aurora phenomenology and show that both radar and spectrophotometer characterization of the precipitating electron fluxes and the response of the ionosphere during these phenomena provide useful data relevant to DNA/AFGL program goals; eg., modeling spatial and temporal irregularities in the excitation and emission of the atmospheric in several visible and IR bands of interest, modeling the temporal response of the atmosphere to transient precipitating electron fluxes, and extending the range of cross calibration between radar and photometric measurements of equivalent quantities related to electron precipitation and ionospheric response for both optical and electromagnetic degradation model applications.

PREFACE

This is the final technical report on contract DNA 001-77-C-0329 covering the reporting period 1 January, 1979 through 27 December, 1981. The purpose of the research funded by this contract was to provide ground based spectrophotometric measurements of auroral and airglow emission intensities in several spectral passbands, and to coordinate these measurements with rocket and aircraft-borne experiments conducted by Defense Nuclear Agency and the US Air Force Geophysical Laboratory.

The experimental program was conducted at the LMSC optical research site located at Chatanika, Alaska. This site is co-located with the SRI International incoherent radar facility. Analytical and supporting tasks were conducted at the Lockheed Palo Alto Research Laboratory.

The principal investigator for this project is R. D. Sears, a member of the Electro-Optics Laboratory. Engineering support was provided by Mr. D. Hillendahl. The cooperation and assistance provided at the Chatanika research site by SRI International personnel; principally, Mr. Dean Feken, the radar site engineer, and Drs. R. R. Vondrak and J. Kelly is gratefully acknowledged. Encouragement and support of our DNA contract officer, LtC. D. W. McKechney (RAAE) is also gratefully acknowledged.

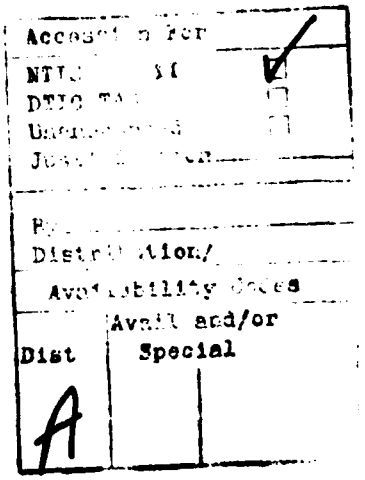

TABLE OF CONTENTS

LIST OF ILLUSTRATIONS

LIST OF ILLUSTRATIONS (Continued)

LIST OF TABLES

1. EXECUTIVE SUMMARY

1.1 Purpose of the Program

Ground based spectrophotometric measurements of auroral and airglow emission intensities were made at the Chatanika optical research site during several observing windows in the reporting period. The purposes of these measurements were:

- o Provide ground based support to DNA and AFGL rocket and aircraft measurements of auroral spectral emissions
- o Obtain coordinated ground, aircraft, rocket, and satellite measurements of the spatial and temporal emission phenomenology relevant to constructing predictive models of infrared emission intensities and structure in several bands of interest to actual or prospective systems
- o Continue coordinated measurements with the Chatanika incoherent scatter radar in order to improve the accuracy of cross calibrations for mutually derived auroral and ionospheric parameters. The goal was to extend this cross-calibration capability over a wide range of auroral intensity and morphological conditions.

1.2 Relationship of the spectrophotometric measurements to DNA Program Requirements

A number of advanced sensor systems require predictive models of infrared radiance in the vicinity of the earth limb over a wide wavelength interval, and over a very wide range of natural and nuclear burst-induced conditions. In addition to prediction or characterization of the mean spectral radiance levels in several important infrared bands, one must be able to determine the spatial and temporal behavior of the spectral emissions, eg., their spatial and temporal power spectral densities (PSD's) and the impact of these quantities upon realistic system models.

The ground based spectrophotometric measurements conducted at Chatanika

PRECEDING PAGE BLANK-NOT FILMED

are directed specifically at the following relevant areas:

- o Determination of the horizontal and vertical distribution of energy deposit in the atmosphere by precipitating electrons under a variety of auroral conditions. These data apply directly to construction of IR radiance models.
- o Determination of the temporal PSD's of auroral spectral radiance in the visible by ground based measurements and extension of these results to several infrared bands. These measurements supported rocket borne IR measurements in several bands of importance to systems applications.
- o Determination of the spatial PSD's of auroral spectral radiance in the visible and near infrared. Application of these data to IR excitation and emission models will provide the beginnings of an auroral and airglow data base characterizing IR emission irregularities observed by scanning and staring sensors.
- o Extension of the radar-photometer cross calibration experiments to a greater range of auroral and ionospheric phenomenology. This capability will allow photometric measurements to substitute for incoherent scatter measurements of certain auroral and ionospheric quantities after the radar is moved from its present location at Chatanika.

Table 1 illustrates the extent of ground based photometric support which has been provided to the DNA/AFGL rocket program in Alaska since the commencement of the ICE CAP Program in 1972.

1.3 Task Summary

This report covers the implementation and results of three contractual tasks for the reporting period. These tasks are summarized as follows:

TABLE 1

GROUND BASED SPECTROPHOTOMETRIC SUPPORT
TO DNA/AFGL ROCKET EXPERIMENTS

Date	Launch UT	Rocket Experiment
3-6-72	1214	OH Photometer
3-9-72	1052	CVF IR Radiometer
3-21-73	1011	OH Photometer (Quiet condition)
3-22-73	1213	CVF, LWIR Radiometer
3-24-73	1031	Multipayload, SWIR
3-27-73	0938	CVF, SWIR Radiometer
2-21-74	0916	HIRIS, LWIR Interferometer
2-25-74	0738	CVF, SWIR Radiometer
3-4-75	0740	OH Radiometer
3-10-75	0912	LWIR Radiometer
3-11-75	0633	E-field Rocket
3-12-75	0748	Multipayload
4-13-75	0946	EXCEDE
2-28-76	0547	EXCEDE
11-19-76	0406	EXCEDE
11-26-76	1025	WIDEBAND
11-13-77	0855	Field Widened Interferometer
2-28-78	0811	WIDEBAND-Multi
10-26-78	0914	SWIR/TMA
10-29-78	0502	EXCEDE II

- o Task 10: The contractor will operate the photometric apparatus at the LMSC/DNA site at Chatanika, Alaska in support of DNA field measurement programs.
- o Task 11: The telescoped multibeam photometer and other photometric instrumentation will support the infrared measurements program and will be coordinated with rocket and aircraft experiments through AFGL.
- o Task 12: Data obtained during the operation(s) will be reduced and applied to the definition of the spatial and temporal PSD's of auroral excited emissions during a variety of conditions. Applications to nuclear excited infrared emission structure will be stressed.

Each of these tasks were completed successfully with the exception of the aircraft-coordinated measurements. Ground based photometric support was not provided to the aircraft experiments during this contract period because of aircraft scheduling problems. The AFGL aircraft ultimately conducted its measurement program in the eastern Canadian sector.

1.4 Experimental Approach

A succession of experiments supported by DNA in Alaska has led to development of a very versatile set of ground based visible and near infrared spectrophotometric instruments. These instruments include:

- o Meridional Scanning (3 color) Photometer (MSP), which measures auroral emission intensity in three spectral regions as it scans along the geomagnetic meridian
- o Three Beam Photometers (3B) which monitor the motion and structure of auroral emission in a single wavelength using three losely spaced fields of view.
- o Multi-beam Telescopic Photometer (MTP), which is a three beam photometer utilizing a large Cassegrain telescope as an objective element in order to obtain very high spatial resolution.

- o Photon-counting digital data acquisition and control system, which acquires the spectrophotometric intensity data in a photon-counting mode, formats the data and records it on magnetic tape. This system also controls the MSP scanner and other system functions.

A summary of the operating parameters of these instruments is contained in Table 2.

TABLE 2

INSTRUMENTATION PARAMETERS

AURORAL STRUCTURE EXPERIMENT

INSTRUMENT	PURPOSE	OPERATING PARAMETERS
MSP	Map auroral conditions in magnetic meridian	Wavelengths, 427.8, 557.7, 630. nm
3B1	Large Scale Structure Spatial,Temporal PSD's	Wavelength, 427,8 & 557.7 nm.
MTP *	Small Scale Structure	Wavelength, 427.8 & 557.7 nm.

COORDINATED RADAR-PHOTOMETER EXPERIMENT

MSP	Very accurately calibrated measurements of auroral emission intensities vs. time	Radar and Photometer boresighted at geomagnetic meridian. Wavelengths, 427.8, 557.7, 630. nm.

Note: * indicates that MTP data was reported in a previous report on this contract.

A fairly comprehensive set of data analysis routines has been developed on previous DNA-sponsored programs. These routines allow interpretation of

spectrophotometric data obtained by one or more of the optical instruments to be interpreted in terms of parametric descriptions of auroral precipitation intensity, its spatial and temporal behavior, and its effect upon the ionosphere. Auroral and ionospheric quantities which have been derived successfully from spectrophotometric data are described in Table 3.

In order to obtain the quantities discussed in Table 3, a variety of software for on-line data reduction, hardware, and computer codes have been developed. A summary of the computer routines used to analyse the spectrophotometric data is contained in Table 4. It should be noted that some features of these codes are proprietary. During the present reporting period, evolutionary improvement of several of the analytical routines was undertaken in order to produce results related to temporal and spatial PSD's which are more responsive to DNA data requirements. During this undertaking close coordination was maintained with some of the eventual users of the spectrophotometric data.

1.5 Field Operations Summary

During the period covered by this report, the ground based photometric apparatus at Chatanika was operated during four separate occasions. Unusually severe weather conditions; severe snow and cloud cover precluded successful operation during two of these attempts, however two successful measurement sessions were obtained, one in each winter observing period (February, 1979, and February, 1980). During the two main observing periods, it was not possible to complete coordinated experiments with DNA/AFGL rocket launches because of rocket launch difficulties and scheduling time; however numerous satellite passes were covered for the DNA WIDEBAND, DMSP, and S3-3 experiments. These passes, plus two sets of passes which were obtained fortuituously during the November 1978 observing window are listed in Table 5.

Ground based data for several DMSP passes were provided to Dr. R. M. Nadile (AFGL) and to Dr. I. Kofsky (Photometrics, Inc.) for furthur analysis. As of the date of this report, a large quantity of ground based spectrophotometric data which is coordinated in time with satellite passes remains to be analyzed.

TABLE 3

SPECTROPHOTOMETRIC MEASUREMENTS:

DERIVED AND INFERRED QUANTITIES

MEASURED QUANTITIES

Photometric Intensities vs. Time (MSP)

A1	427.8 nm	N_2^+	E-Region
A2	486.1 nm	H	F- and E-Regions
A3	557.7 nm	$O(^1S)$	E-Region
A4	630. nm	$O(^1D)$	E- and F-Regions

Photometric Intensities vs. Time and Space (3B and MTP)

B1	427.8 nm.	N_2^+	E-Region
B2	557.7 nm.	$O(^1S)$	E-Region
B3	589. nm.	Na	E-Region
B4	630. nm.	$O(^1D)$	E- and F-Regions
B5	Near IR	OH	D-Region
B6	Near IR	$O_2(^1\ )$	D-Region

DERIVED QUANTITIES

C	Energy Deposit by Precipitating particles	from A1
D	Flux of Precipitating Protons	from A2
E	Photometric Intensity Ratios	from A1,A3, A4
F	Temporal PSD's	All spectral emissions
G	Spatial PSD's	All B- measurements
H	Related Statistical Quantities	All above

INFERRED QUANTITIES

J.	Mean Energy of Precipitating Electrons	from E
K.	Auroral Electric Fields	from B, H
L.	Ionospheric Electron density, conductivity	from B, E
M.	Precipitating Electron Number Flux	from B, E

TABLE 4

COMPUTER ROUTINES USED FOR PHOTOMETRIC DATA ANALYSIS

Data Reduction	COPY
	EDIT
Spectrophotometric Analysis	CAL7, CAL 10
	NUCAL
	CALX
Structure Analysis	NUWAV(7, 10, 11)
	POWSPC
	POWDEN
	NUPSPC
	PLOTSM
	AUXCOR
	LSTSQR
	CHAP 8

Table 5 SATELLITE PASSES COVERED.

Date	Time	Satellite
11-11-77	0900	WIDEBAND
	1030	WIDEBAND
11-12-77	0940	WIDEBAND
11-13-77	1010	WIDEBAND
2-28-78	0952	WIDEBAND
3-1-78	0846	WIDEBAND
	1031	WIDEBAND
3-2-78	0926	WIDEBAND
3-4-78	0820	WIDEBAND
10-26-78	1037 UT	DMSP
10-29-78	0831	WIDEBAND
10-31-78	0950	WIDEBAND
	1031	DMSP
11-1-78	1014	DMSP
	1030	WIDEBAND
11-2-78	0925	WIDEBAND
	0956	DMSP
	1110	WIDEBAND

During the two best observing windows, February, 1979 and February, 1980, two sets of coordinated measurements were made at Chatanika using the spectrophotometric instruments and the incoherent scatter radar. During the 1979 window, emphasis was placed upon deriving auroral emission spatial and temporal PSD's from the photometric data. During the 1980 window, the goal was to observe intense pulsating aurora simultaneously with the optical and radar instrumentation, but an unexpected opportunity to study the detailed phenomenology of the auroral precipitation and ionospheric response on the poleward edge of the auroral region during intense activity conditions presented itself.

Field program and data handling procedures may be summarized as follows:

- o Operation of the photometric apparatus is maintained during every cloudless night regardless of the status of potential collaborative, or supporting experiments; eg. radar, rocket launches, aircraft schedules, or satellite passes.
- o All instrumentation is subjected to both manual and automatic calibration at the beginning and end of data runs: more often if required.
- o All coordinated experiments are cross-logged and times coordinated to the nearest second.
- o All data for cloud-free observing periods are translated into library tapes and editing copies run in order to assess data quality and applicability to DNA program goals.
- o A data synopsis sheet is completed for each successful night of operation.

Data synopsis sheets for the experimental periods covered by this report are labelled "AGIN-XX" for the 1978-79 period, and "PULSE-XX" for the 1979-80 interval. These sheets are contained in Appendix A to this report.

1.6 Summary of Results

Coordinated radar and optical measurements of auroral precipitation and the response of the ionosphere to this disturbance show that a number of useful

quantities may be derived from both radar and photometer measurements. Temporal and spatial PSD's of the irregularities in auroral precipitation have been measured over a wide range of pre- and post-breakup conditions. Analytical models such as BRIM may be used to relate these PSD data to equivalent spatial and temporal fluctuations in several IR bands of interest. Likewise, coordinated optical spectrophotometric and radar measurements have extended the intensity and phenomenology range over which independent measurements of auroral and ionospheric parameters,such as total energy deposit, the mean energy of the precipitating electron flux, spatial and temporal fluctuations of the precipitating flux, electron density vs. altitude, the height-integrated Pederson and Hall conductivities in the auroral ionosphere, and dynamical details relating to the ionospheric response to impulsive, pulsating, and drifting patches of auroral precipitation may be made with confidence. All of these quantities contribute vital input to predictive models of IR excitation and emission during natural and nuclear-burst conditions, as well as to models of the response of the ionospheric electron density in three dimensions to natural and artificial disturbances. As such, these data may provide a useful data base against which to test some of the predictive codes such as ROSCOE, WOE, etc.

2. MEASUREMENTS OF AURORAL EMISSION STRUCTURE

2.1 Experiment Summary

Spatial and temporal PSD measurements of auroral emission structure were made using the three beam (3B) photometers during active auroral periods. Auroral structure measurements were made in two different wavelengths, 427.8 nm which is emitted promptly from the N_2^+ ion and 557.7 nm, which is emitted by the $O(^1S)$ state. Although the oxygen excited state, ^1S has an approximately 1 sec. lifetime, temporal and spatial PSD's over the frequency and spatial ranges considered herein are essentially identical. Therefore, all data presented in this section represent PSD's computed from $O(^1S)$, 557.7 nm measurements because of a somewhat greater signal to noise ratio in the measurements. The geometry of the three beam photometer measurement is illustrated in figure 1. The characteristics of the three beam instruments are described in the next section.

The analytical basis for the multibeam photometer structure measurements depends upon cross correlation and power spectral density analysis of the intensity fluctuations observed in each of the three spaced fields-of-view. The intensity irregularities are modeled as a superposition of plane waves passing through the fields of view of the instruments. Details of the analytical techniques are contained in previous DNA reports (see references 5, 6, &9) and are summarized in a following section.

2.2 Instrumentation

Three photon-counting, three channel spectrophotometric instruments were available to conduct the auroral emission structure experiments: two three beam instruments and the meridional scanning photometer. A total of nine photon count channels plus a digital clock readout of Universal Time is fed to the data system as illustrated in figure 2. The system integration time is one second and the data block length is 300 seconds.

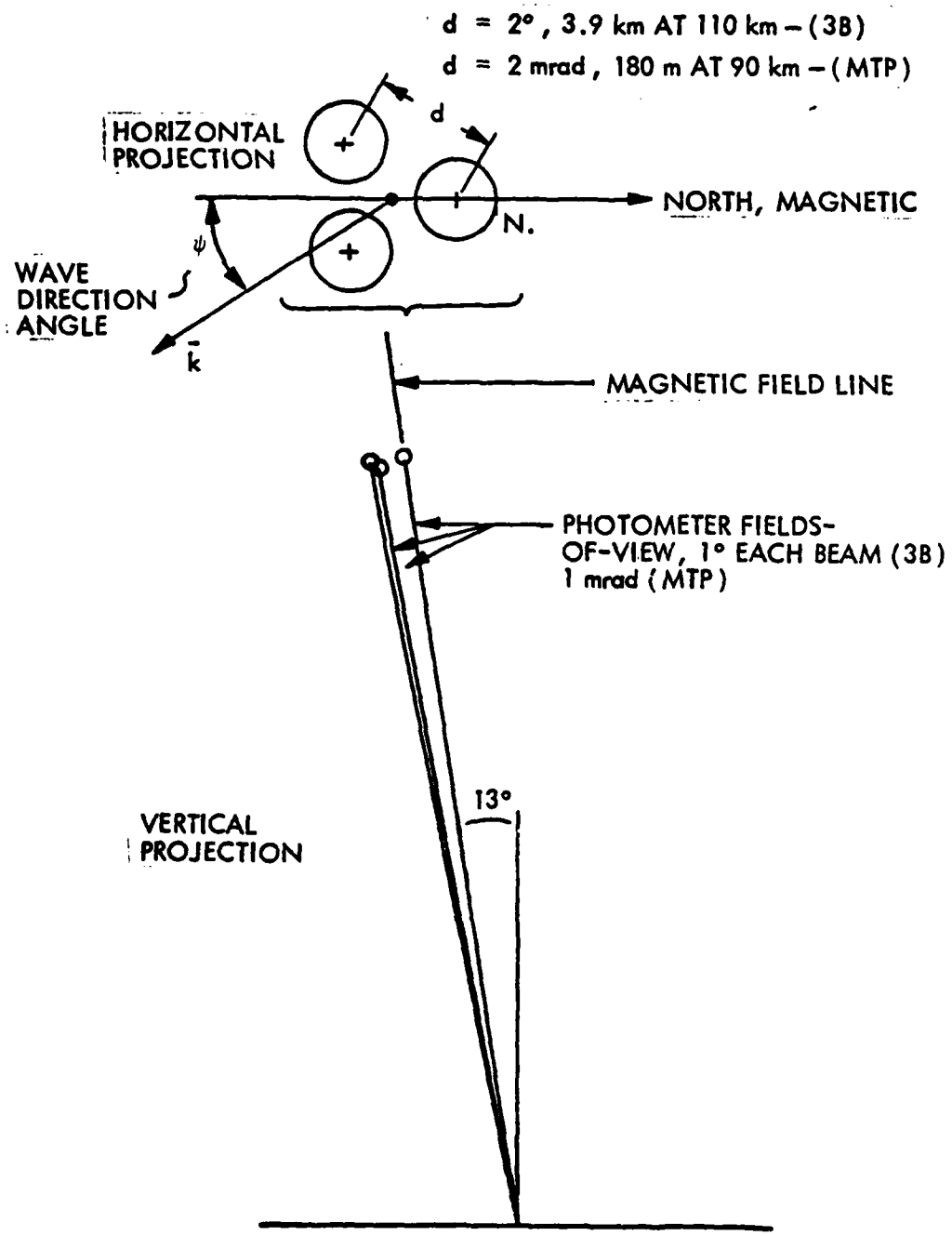

Figure 1 Geometry of the three-beam photometer experiment

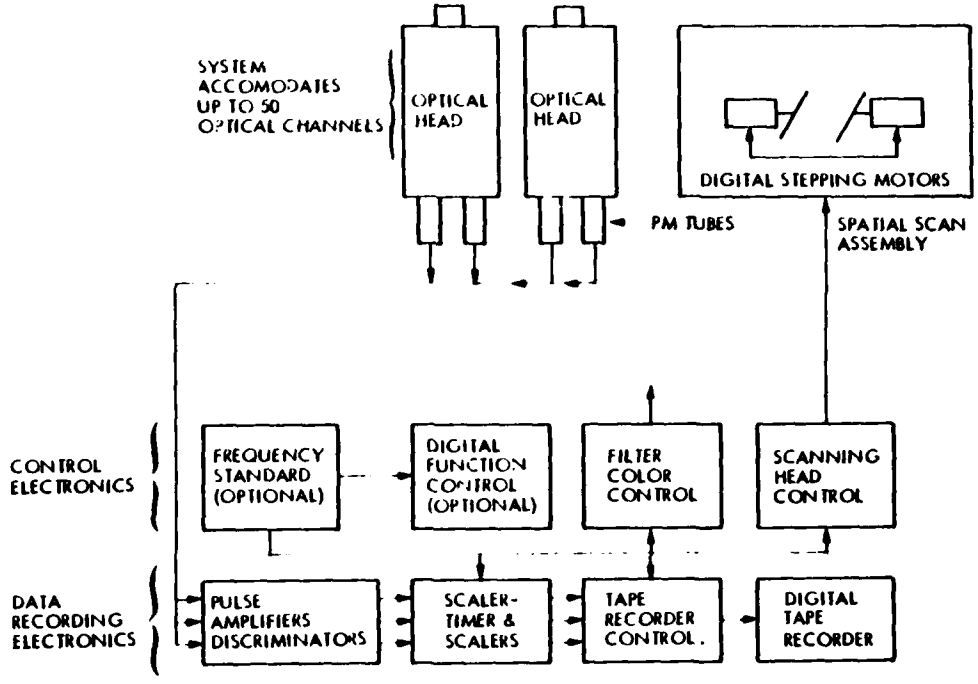

Figure 2 Digital data acquisition and control systems for photon-counting spectrophotometers

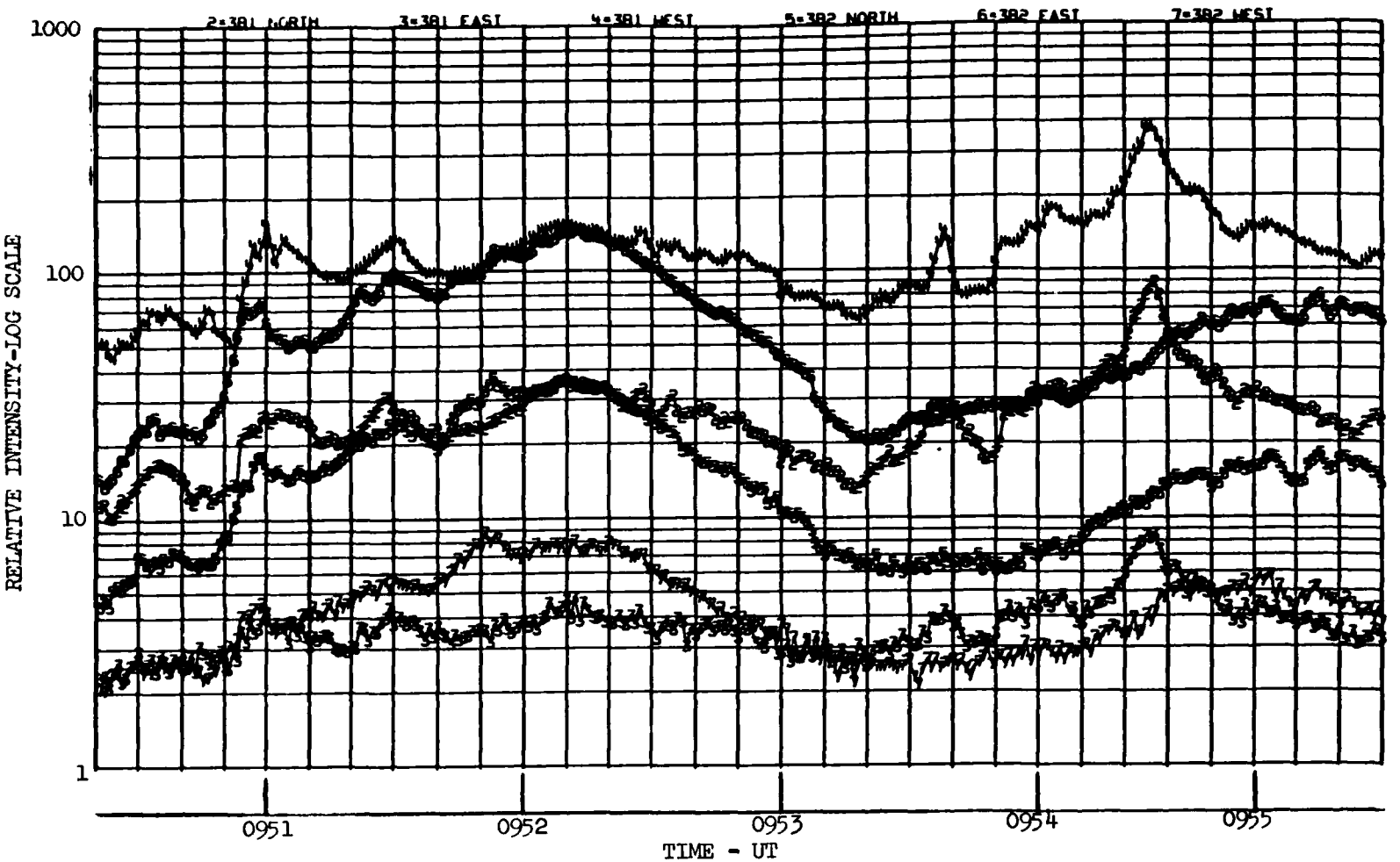

Figure 3 Example of a five minute data segment from two three-beam (3B) photometers.

Although the electronic pulse counting and recording system is common to all of the optical instruments, the application and characteristics of each optical head differ significantly. The operational parameters for the optical instrumentation is summarized in Table 6. Here, it should be noted that the MTP (Multibeam telescoped potometer) was operated only during the 1978-79 observing period. Data from this instrument are reported in reference 7 . Each of the instruments described are modular derivitives of the three color photometer system described in reference 7.

TABLE 6

PHOTOMETER OPERATING PARAMETERS

PARAMETER	MTP	3B	MSP
Wavelength	427.8	427.8	427.8
	557.7	557.7	557.7
			630.
Field of View (Each beam)	1mrad.	17 mrad.	50 mrad.
Spatial Resolution	300m.	6 km.	5 km
Orientation	Zenith	Zenith	Meridional Scan

An example of a data stream received from two of the multibeam photometers during an active aurora is illustrated in figure 3. The time interval covered is 300 seconds. These data represent the raw count rates received by the data system during passage of an auroral band through the fields of view of the 3B instruments. All data are previewed in this manner.

2.3 Analytical Procedure: NUWAV Code

Data analysis for the auroral structure experiment is conducted using a series of UNIVAC codes which are designated NUWAV. This complex sequence of statistical algorithms was developed during the period of DNA support to the Chatanika ground based optical experiments. The concept for this complex of codes and many of the details were developed independently at LMSC for other purposes.

A general flow diagram for the NUWAV code is illustrated in figure 4.

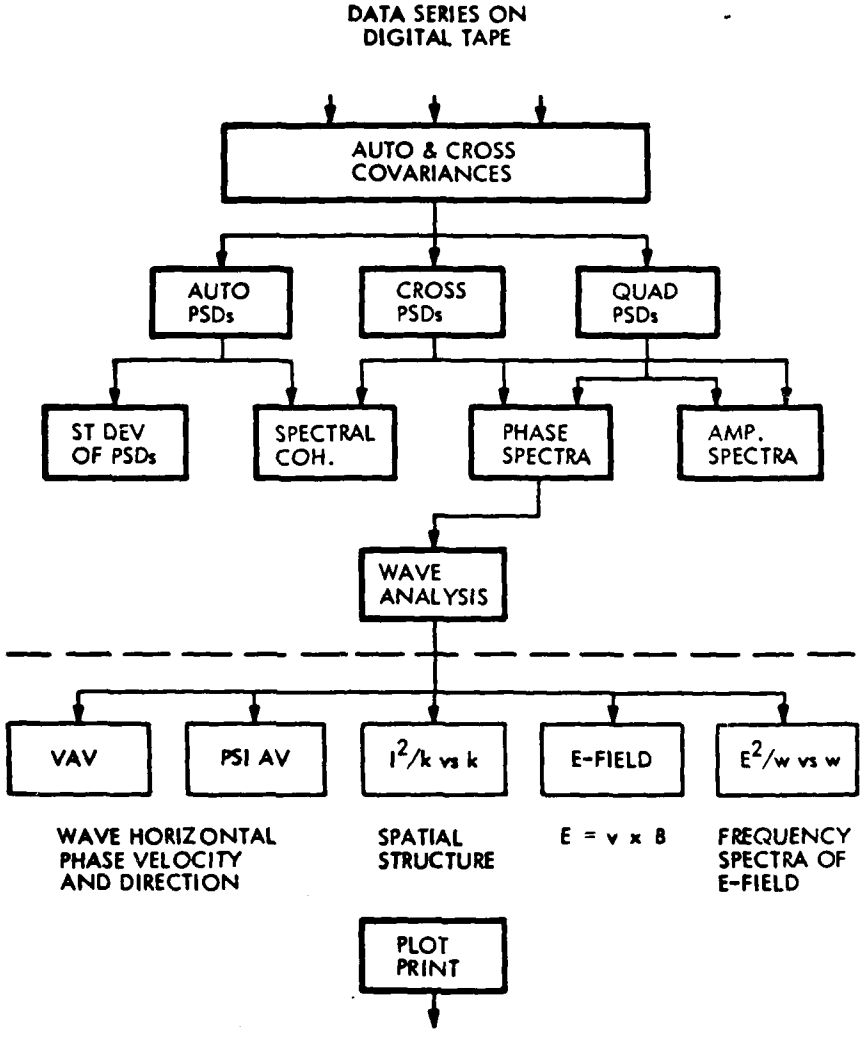

Figure 4 Organization and structure of the NUWAV analysis code

The major change between the code version used herein and versions described in previous DNA reports is the inclusion of an improved data smoothing routine.

The input data stream, three parallel digitized intensity measurements, is detrended and then subjected to the individual computations as illustrated in figure 4. Each computation is performed on the data, block by block, however, it is possible to obtain a greater dynamical range in spatial and spectral PSD's by combining blocks of data. A typical input record, one data block after detrending, is illustrated in figure 5.

After computing the appropriate auto and cross correlation functions, (level 2 in figure 4), the complex temporal PSD components are computed and stored (level 3). The temporal PSD's for each intensity channel are illustrated in figure 6. Each fluctuation PSD spectrum shows a clear power-law behavior at low frequencies with a spectral index approximately f^{-3}. Rolloff at the lowest frequency is caused by the spectral window used (Parzen window). The noise level for this particular set of PSD's is at approximately the 1×10^{-2} level on the plot.

Level 3 data may also be used as qualitative indicators of the data quality. The standard deviations of the computed PSD's as well as the inter-channel spectral coherence of the data is available as an output. Typical values of the PSD standard deviations are about 20 to 30 percent at the $\gamma = 1$ level. In practice, the spectral coherence value is used to filter the data for furthur processing: coherence values above 0.7 indicate that the wave analysis may be applied with reasonable accuracy; values between 0.3 and 0.7 indicate useful but somewhat inaccurate data; values below 0.3 indicate that the data are of doubtful accuracy.

The first indication of the motion of auroral forms through the fields of view of the 3B instruments can be obtained by examination of the cross correlation plots in level 2. Figure 7 illustrates cross correlations obtained for the data sample presented in this section. The geometry of the data series is as follows: fov 1 is pointed to geomagnetic north of zenith, fov 2 is to the southeast, and fov 3 is to the southwest. The zero lag between beams 2 and 3 indicate very little E-W motion. Nearly identical time lags (-5 sec.) between pairs 1-2 and 1-3 indicate a N-S motion with an estimated velocity of 1 km. sec. $^{-1}$.

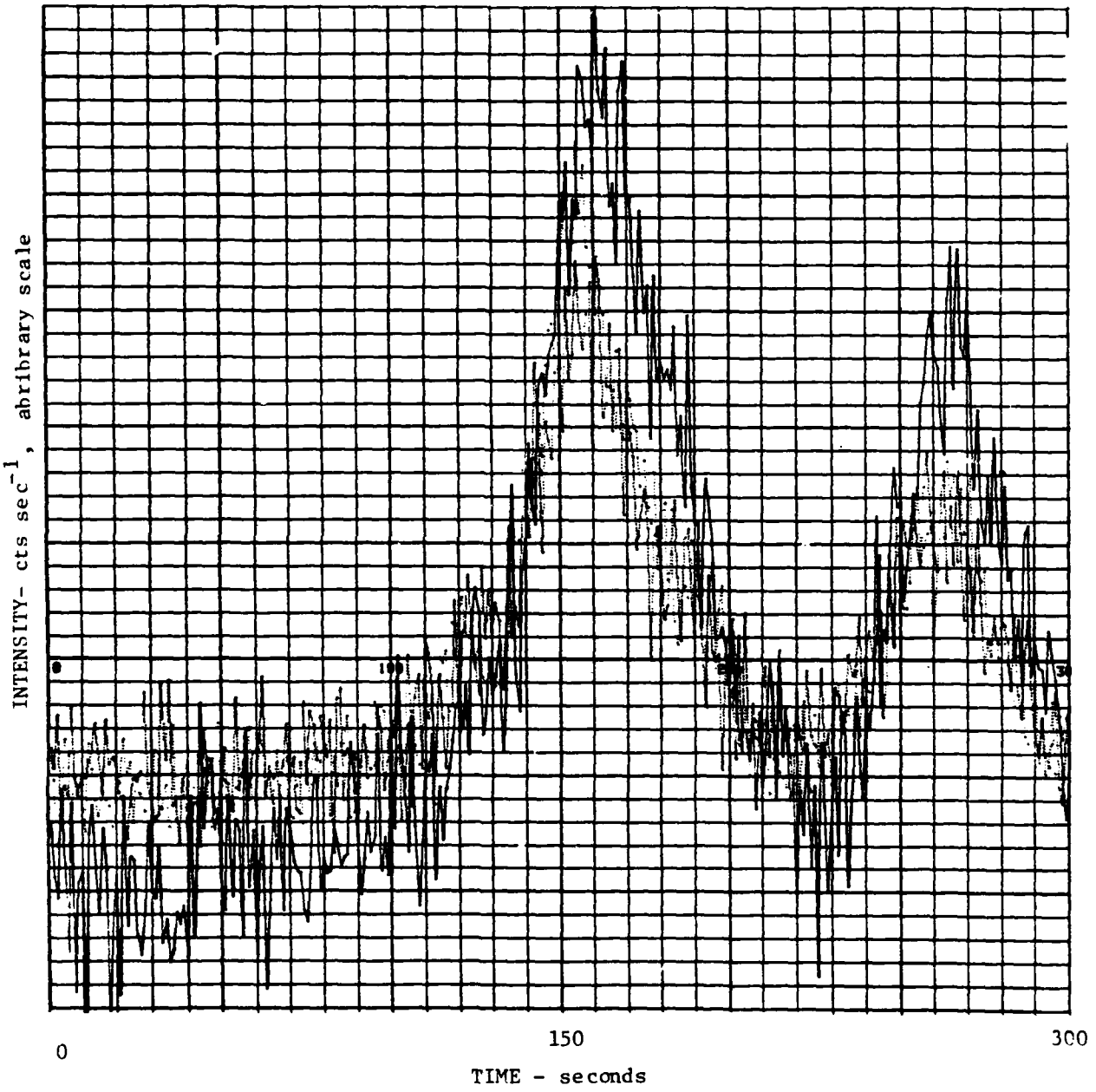

Figure 5 Detrended input data block for NUWAV processing.

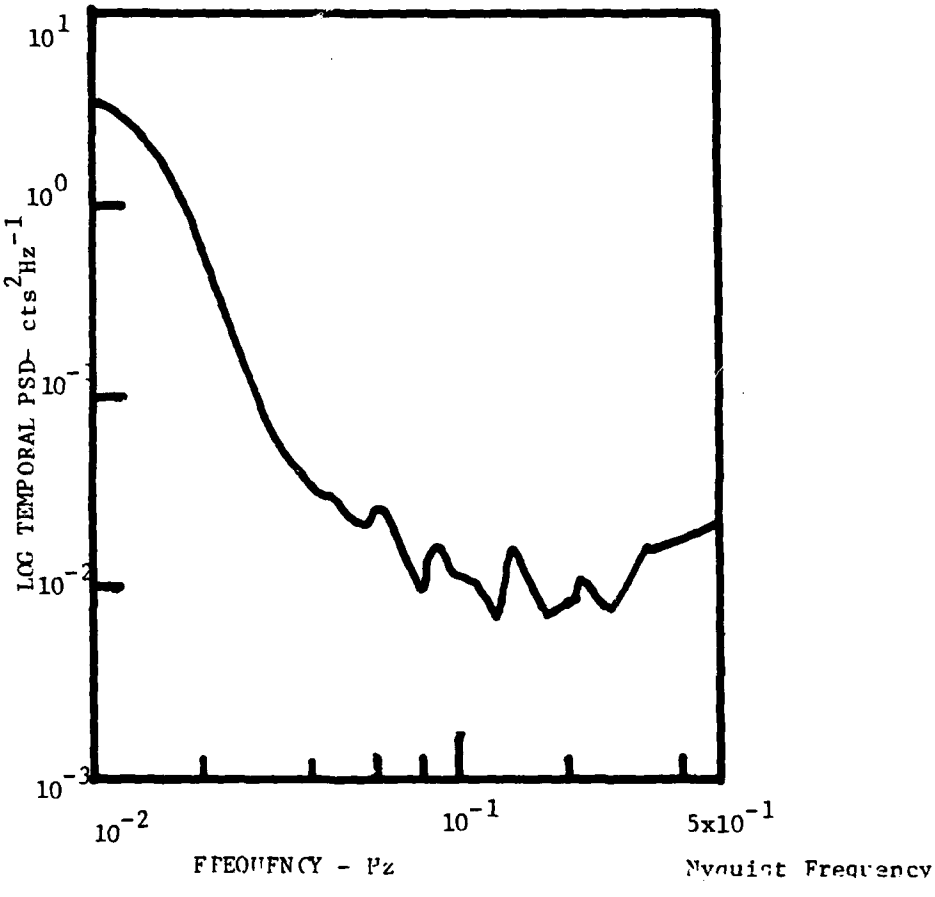

Figure 6 Temporal PSD computation for data block of figure 5 using NUWAV code.

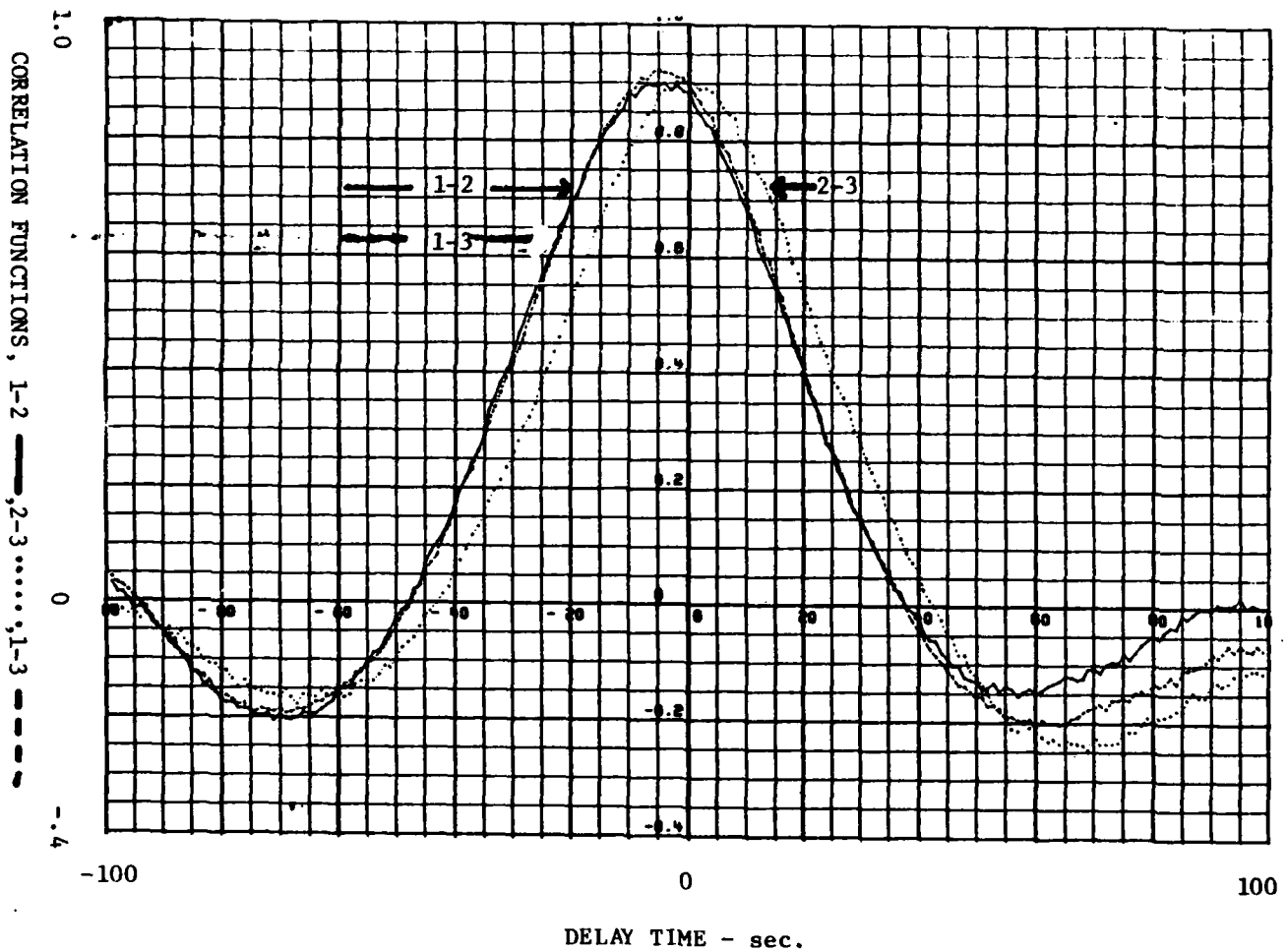

Figure 7 Cross correlation function computed in NUWAV from data block illustrated in figure 5. Reference numbers for each of the three beam pairs are 1-2, N-SE; 2-3, SE-SW; 1-3, N-SW.

The wave analysis section of the NUWAV code (level 4) computes the horizontal phase velocity of a horizontally propagating plane wave as a function of frequency. The algorithm is structured such that a superposition of plane waves is assumed. Several outputs related to this computation are available: horizontal phase velocity vs. frequency, the velocity vector vs. frequency; and the average velocity over the entire frequency window. Because of signal to noise level considerations at the higher frequencies, careful evaluation of the statistical accuracy of these computations must be achieved. In order to evaluate these output data, the cross channel coherence values are checked, and indicators placed on the plots of phase velocity in order to denote high quality, medium quality, and low quality data. Figure 8 illustrates the output of the NUWAV code at level 4 specifically related to the horizontal vector velocity dispersion curves. Two important features of these curves are important to the interpretation of the 3 beam data in terms of auroral intensity fluctuation spatial PSD's. One is the frequency range over which high signal to noise ratios are maintained with consequently high cross-channel coherence, and the other is the tendency of the auroral spectral velocity plots to exhibit dispersive characteristics both in magnitude and in direction. In this regard, figure 8 is typical of most of the auroral emission irregularity computations using the NUWAV code approach. The regions of highest accuracy and statistical confidence in the data (as derived from the coherence value criteria) are denoted on the figure as * (highest confidence level), x (medium confidence level), . (lowest confidence level). Data plots subsequent to this figure will contain data only in the first two confidence categories.

The horizontal phase velocity and vector direction of the auroral emission irregularities are used to derive the spatial frequency of the irregularities in the N-S and the E-W directions. This conversion is accomplished by means of two simple transformations of the display axes:

$$k = 2\pi v/f \qquad 1)$$

and $$PSD(k) = G(v,f)\ PSD(f), \text{ where } G = 2\pi f^2 v^{-1} \qquad 2)$$

These expressions are derived from the dispersion relationship between

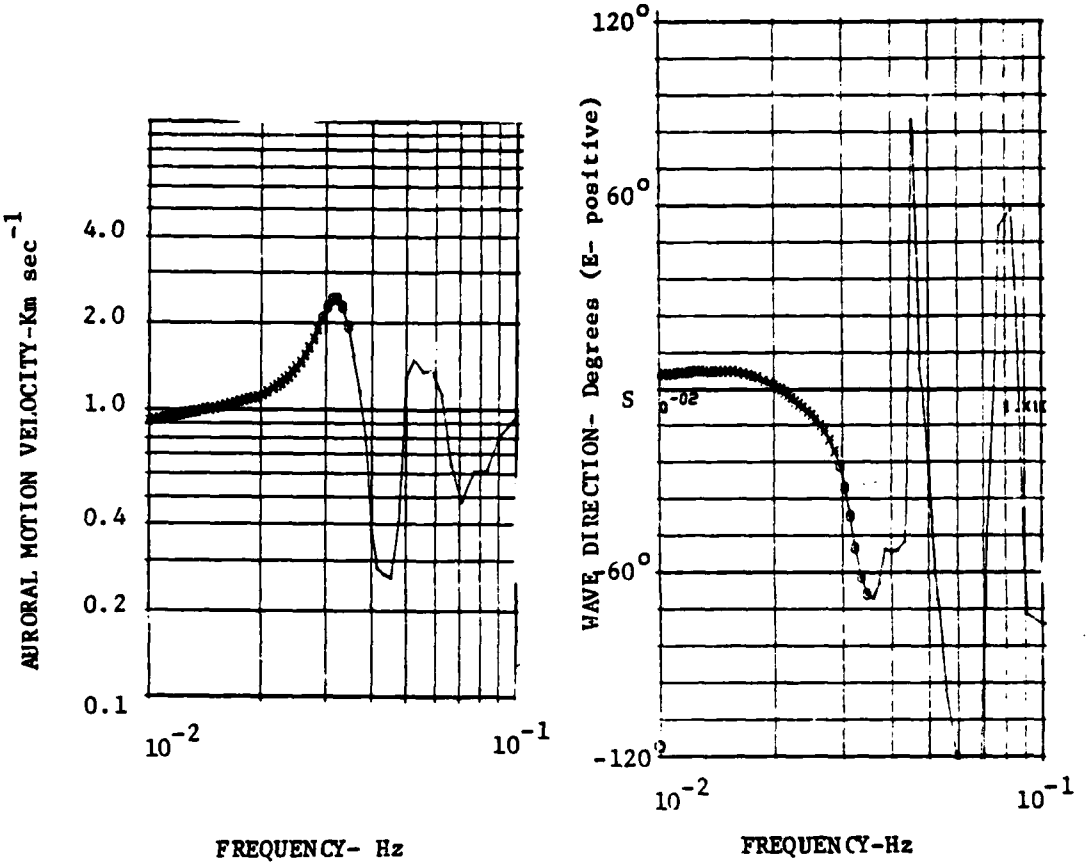

Figure 8 NUWAV code computation of vector velocity dispersion curves for 3 beam data of figure 5. In this figure horizontal phase velocity (km/sec) and vector direction (measured from S) are graphed.

the horizontal wave velocity, v, the angular wave frequency , ω, and the spatial frequency, k. In the cases analysed in the NUWAV code, it is assumed that the horizontal phase and group velocities are the same, but it is recognized that this is an approximation in many cases.

The results of this two dimensional transformation into k space is illustrated in figure 9. Each figure represents the spatial PSD of the auroral emission irregularities in the geomagnetic N-S and E-W directions. With the exception of some computational anomalies on the N-S plot, each spatial PSD shows a power law behavior with index k= -1.3. The spatial frequency regime represented by this data set covers a range 0.1 km^{-1} to about 10 km^{-1}. This range corresponds to a sinusoidal wavelength range of 0.6 to 100 km for the auroral irregularities.

In the next section, a series of spatial and temporal PSD's for a variety of auroral conditions is presented.

2.4 PSD Measurement Results

During the February 1980 observing period, a period of unusual auroral activity was identified and detailed spectrophotometric measurements of the auroral distribution, and its spatial and temporal intensity fluctuations were made. In conjunction with the photometric experiments, the Chatanika incoherent scatter radar was operated during part of this experiment.

The series of spectrophotometer measurements was made between 0500 and 1300 UT on February 16, 1980. This interval was characterized by intense auroral activity and several magnetic substorms. At dusk, auroral activity had already passed the zenith at Chatanika and was observed near the southern horizon. Poleward expansions, magnetic bays, and other activity continued throughout the period of the experiment. Reference to PULSE04 data summary (see Appendix A) indicates that throughout the evening a series of apparently sun-aligned forms was observed. Spatial and temporal PSD measurements reported in this section refer to the temporal development and detailed temporal and spatial PSD's observed for these forms.

The development of the NW-SE aligned forms is illustrated in the photographs displayed in mosaic form in figures 10 and 11. A development

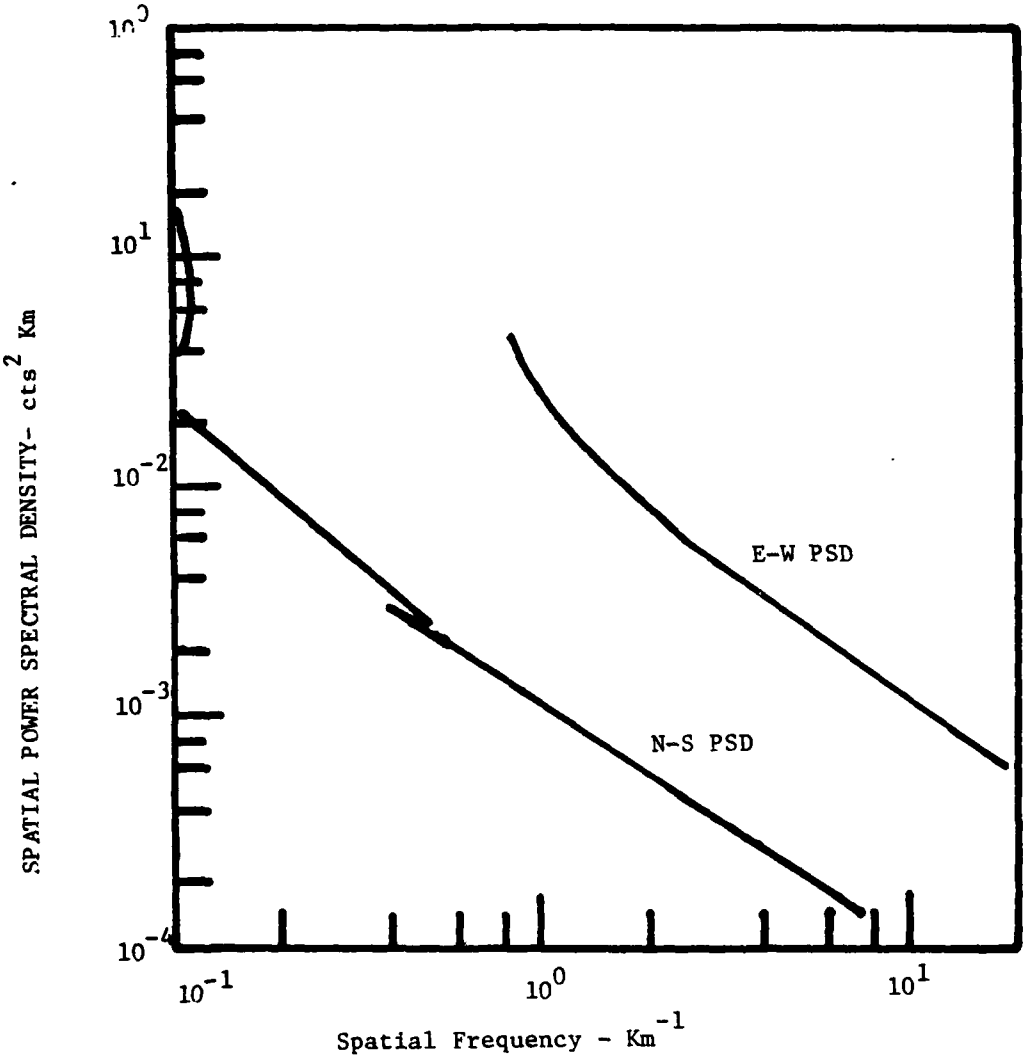

Figure 9 Results of NUWAV transformation of PSD and vector velocity data into orthogonal (N-S) and (E-W) spatial PSD's

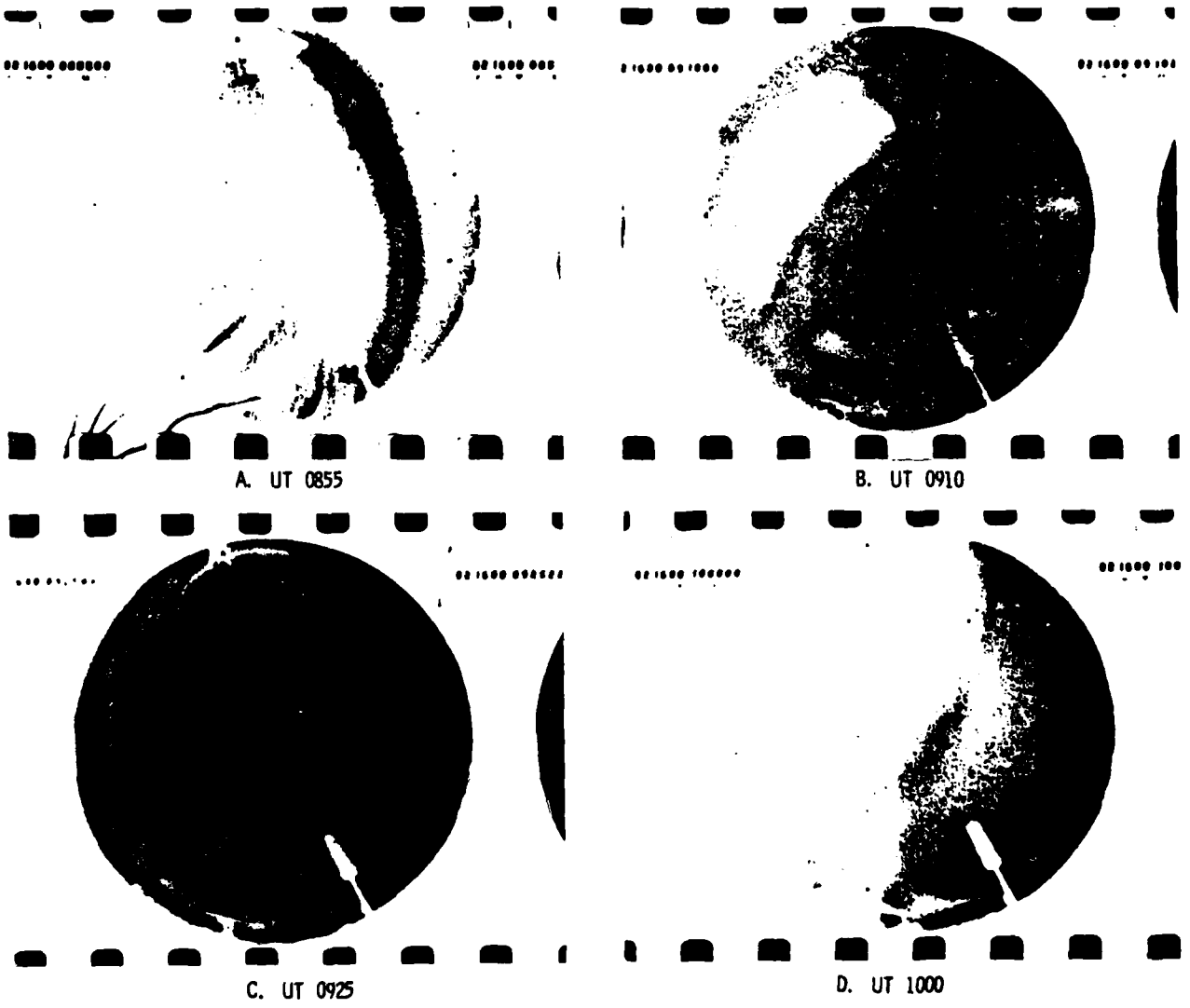

Figure 10 Photomosaic presentation of all sky camera photographs for experimental period on 16 February, 1980.

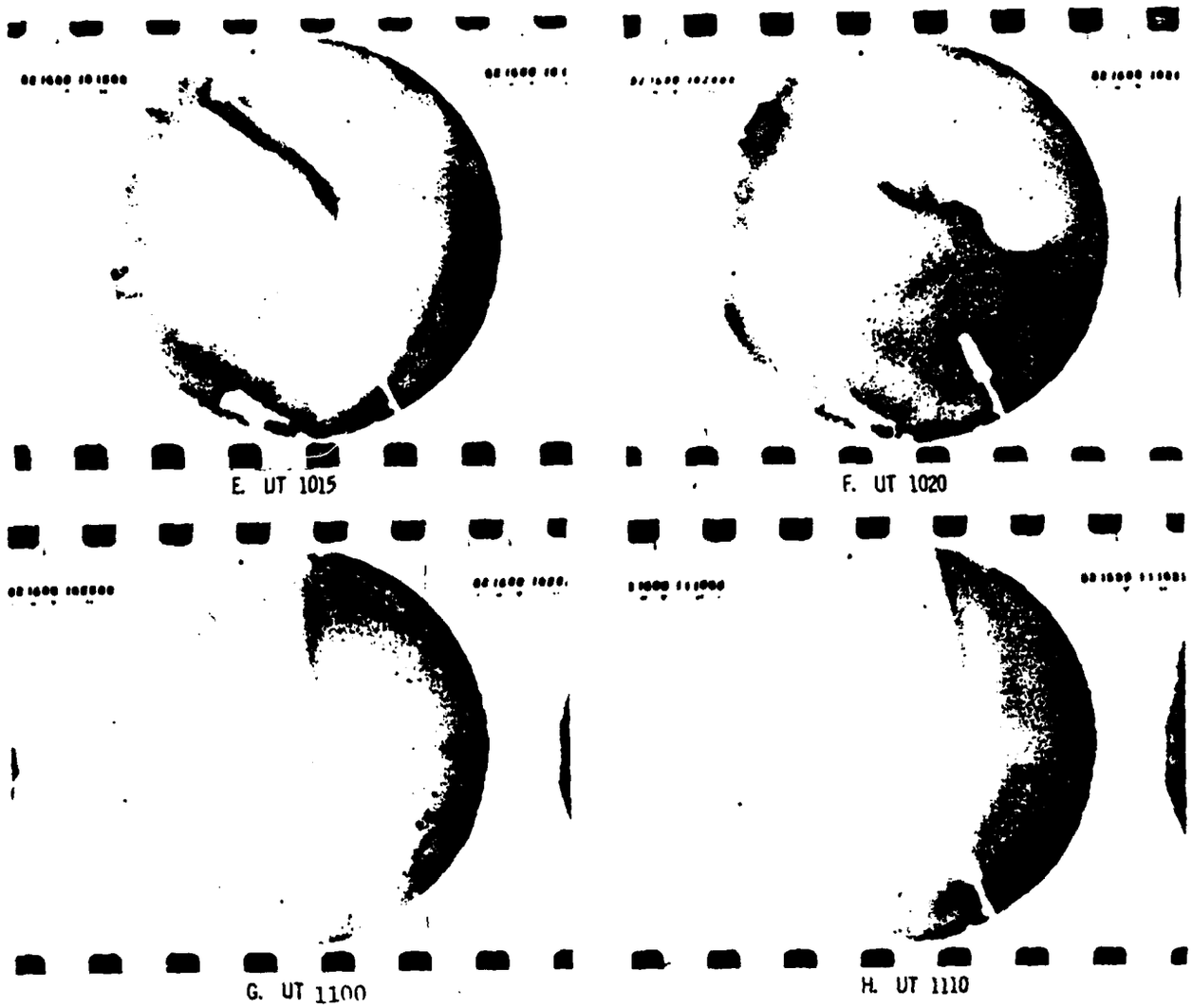

Figure 11 Continuation of data mosaic begun in figure 10.

sequence is illustrated: quiet arc and poleward expansion (panels A, B, and C), relaxation to relative quiet (panel D), development of a NW-SE form followed by a surge (panels E and F), followed by relaxation to relative quiet (panels G and H). Other similar sequences were observed later in the evening, however they were too weak to show up well on the second generation all sky camera images. Other measurements related to the temporal phenomenology of the aurora and ionosphere during this period are reported in section 3 of this report.

Without furthur documentation, it is not clear whether the auroral NW-SE structure studied in this section represents a sun-aligned arc characteristic of those observed in the poleward side of the auroral oval, or whether it is characteristic of the Harang discontinuity. Geomagnetic observations from the Alaska sector may resolve this point, but it does not affect the results of the spatial and temporal PSD computations.

Detailed computations of the temporal and spatial PSD's were performed for the period 0900 to 1010 UT on 16 February 1980. This period was chosen for its large signal to noise ratio which should produce optimum PSD results.

The variability of the temporal PSDs which are computed for the period of auroral breakup and poleward expansion (figure 10, panels B-D) is illustrated in figures 12 and 13. The great variability between successive five-minute data samples and their computed temporal PSD's is noteworthy, especially when filter design concepts for staring sensors is considered. An attempt to demonstrate this problem is presented in figure 14, where the mean value of the count rate, the low frequency (0.01 Hz) and the high frequency (0.1 Hz) values of computed PSD's are compared for successive data samples. Figure 14 shows that the mean count rate (directly proportional to radiant intensity) and the low frequency fluctuation power covary at least approximately whereas the high frequency power behavior exhibits excursions of more than a factor of 10 between successive data segments. Points below the estimated mean noise level for the data interval should be ignored. One may obtain a somewhat more quantitative appreciation for the reality of the high frequency power and its statistical accuracy by consideration of the magnitude of the cross channel coherence of the data, which was mentioned previously. The coherence spectrum for panel A is illustrated in figure 15,

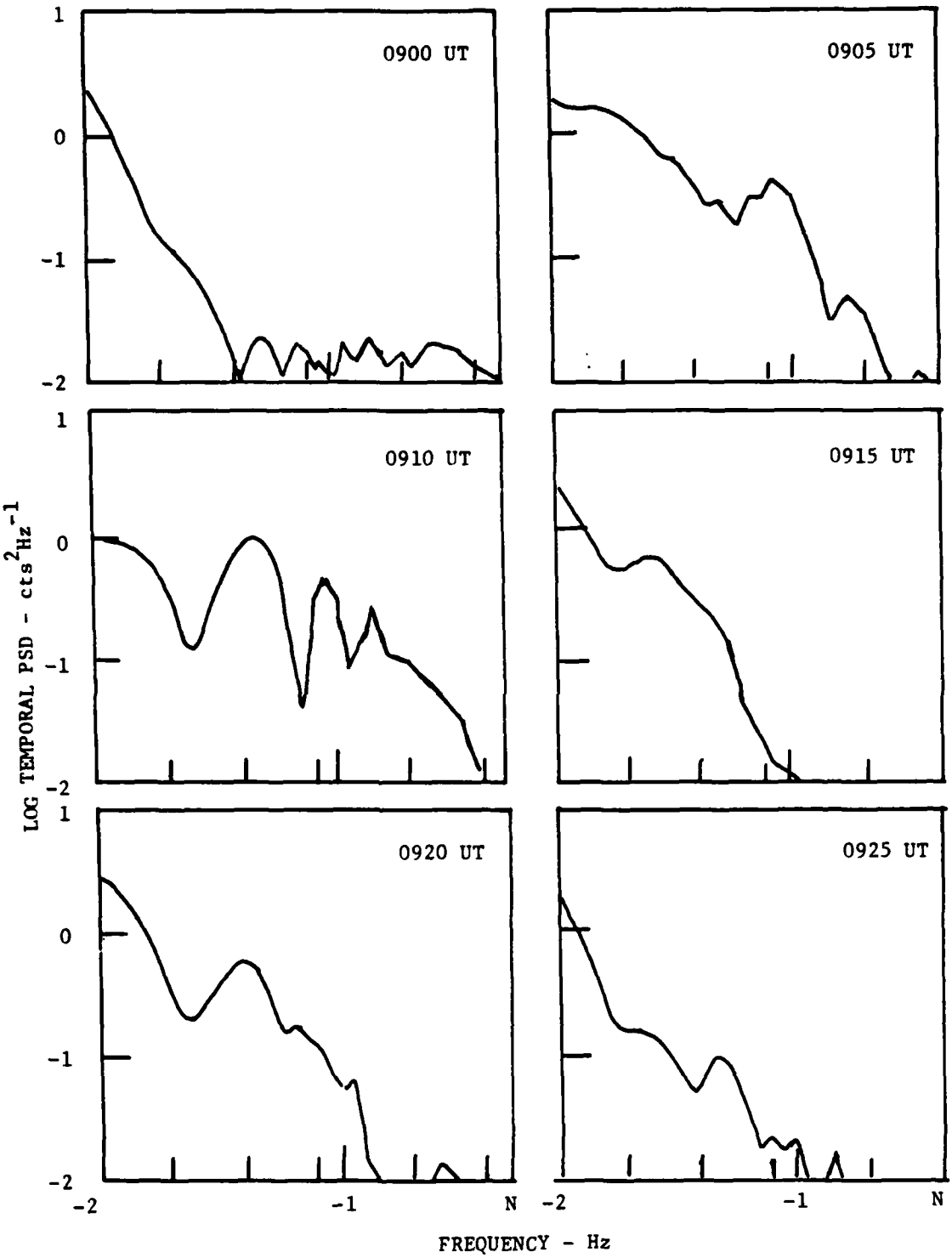

Figure 12 NUWAV computation of temporal PSD's for period 0900-0930 UT, 16 February, 1980.

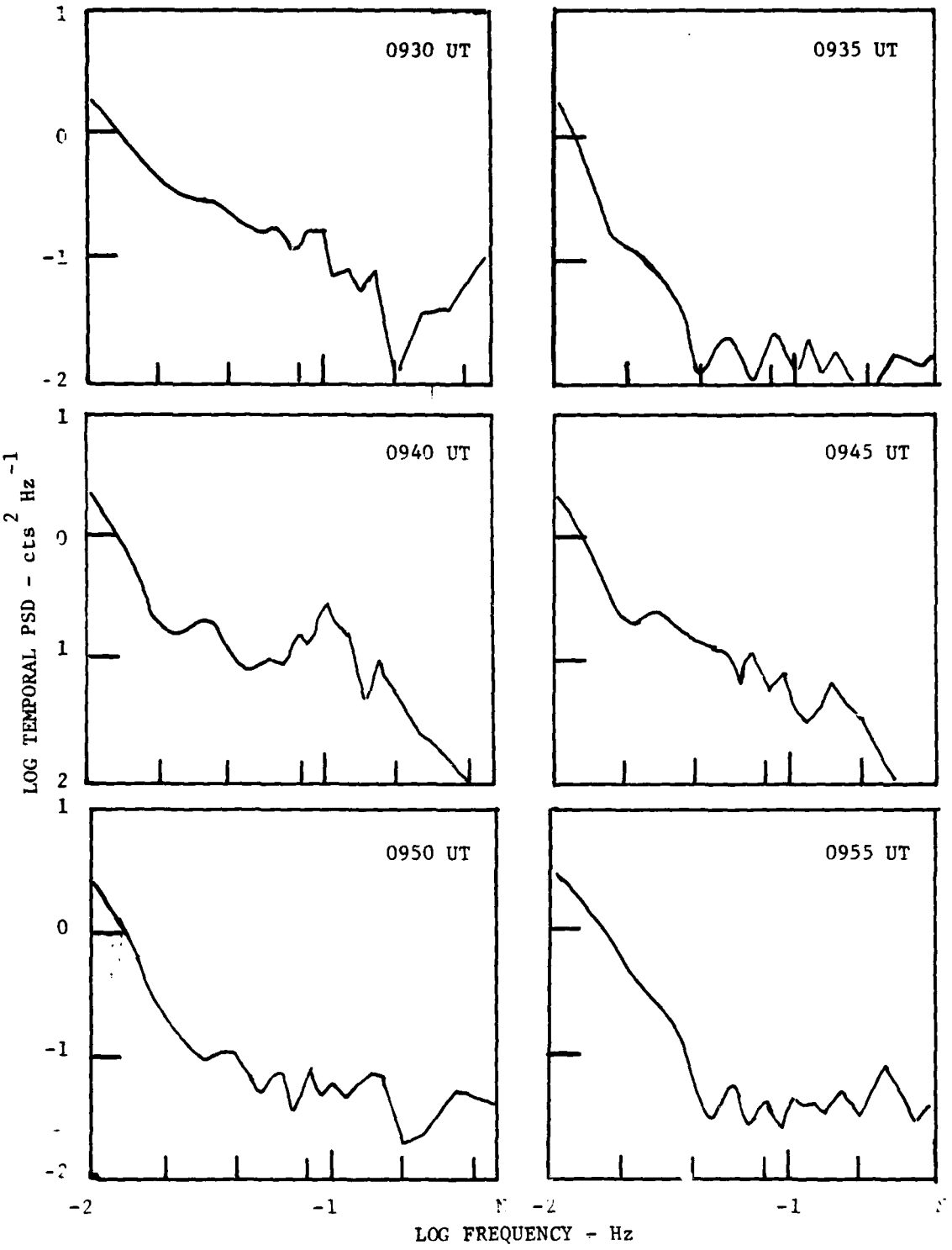

Figure 13 NUWAV computation of temporal PSD's continued from figure 12. Period covered is 0930 to 1000 UT. Nyquist Frequency 0.5 Hz = N.

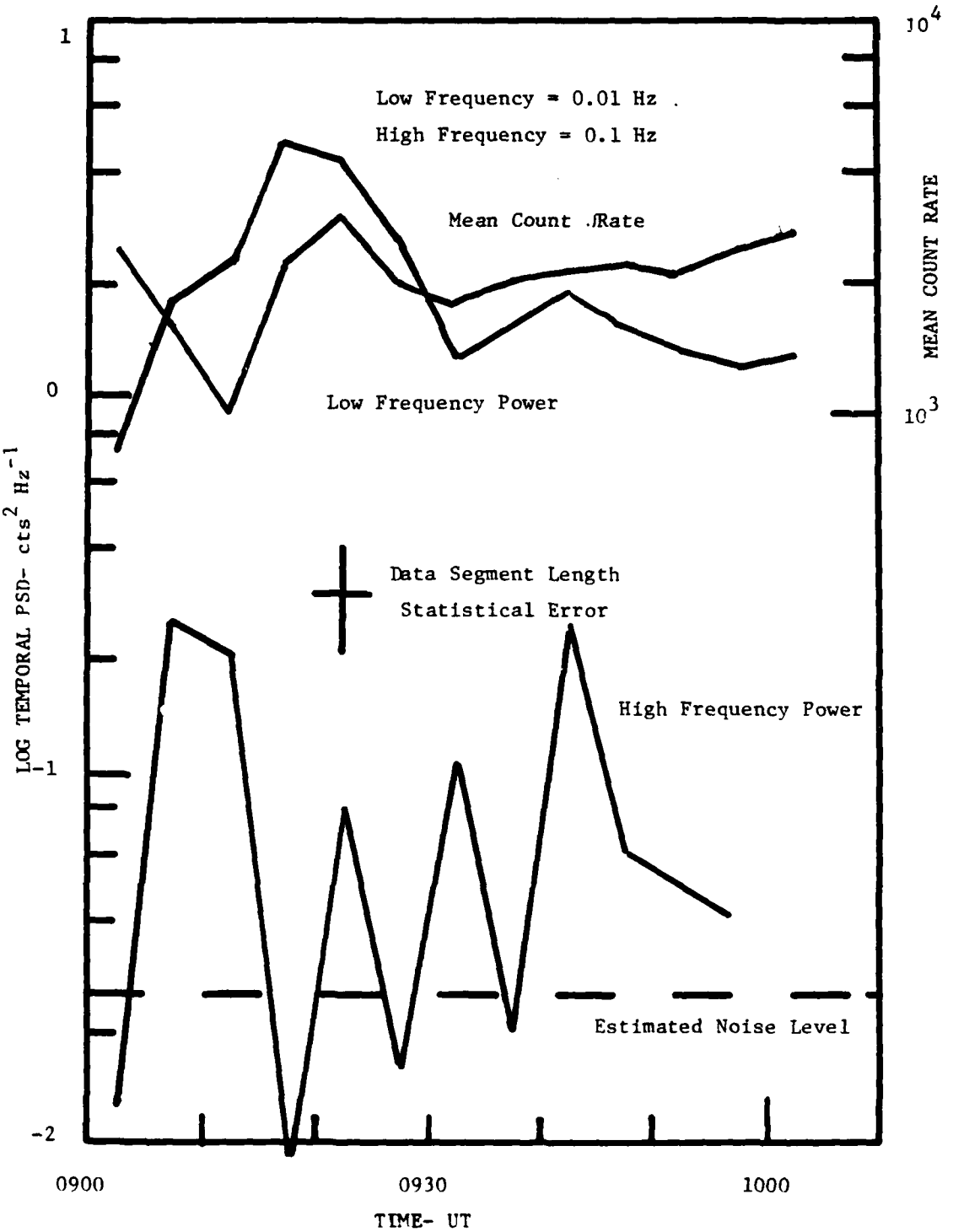

Figure 14 Temporal variations of mean intensity, PSD low frequency component, magnitude, and PSD high frequency component magnitude for data presented in figures 12 and 13.

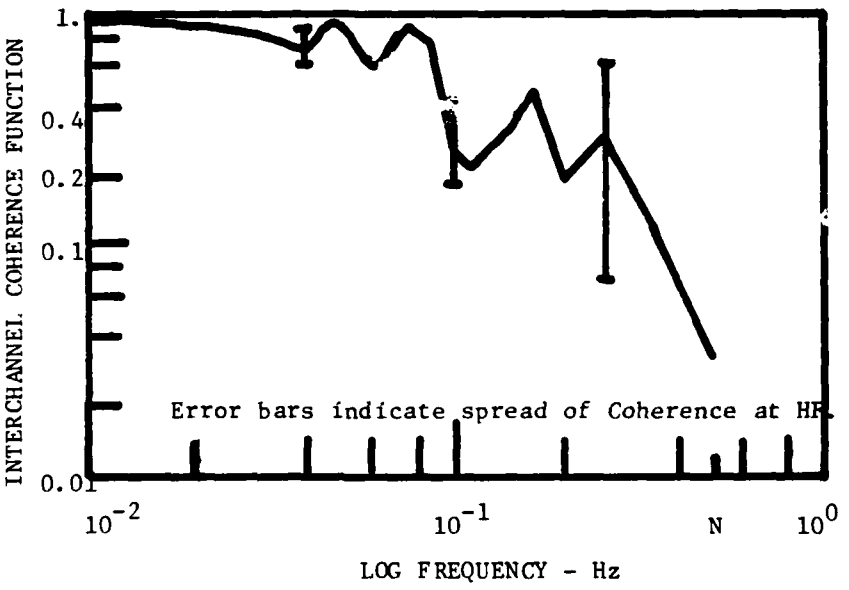

Figure 15 Cross Channel Coherence Function computed by NUWAV.

which shows cross channel coherencies are maintained at or above values of 0.3 to frequencies of 0.1 Hz. The large variability and relatively lower average magnitude of cross channel coherence above 0.1 Hz indicates that the data are noisey. and than PSD and other statistical quantities derived from the data are of low quality.

Some of the temporal PSD's show evidence for auroral pulsations of significant magnitude (see panels B, C, D, E, etc.) which show up in the PSD plots as power enhancements at high frequencies relative to an average power law fall-off with frequency.

An equivalent time sequence of spatial PSD's is illustrated in figures 16-19 for the same time interval covering the temporal PSD plots. All of the spatial PSD's show similar power law behavior. During active times, eg. during poleward expansion, breakups, and passage of auroral arcs, some departure from nominal behavior is observed. Also some computational anomalies such as the hooks at the low frequency end of the plots are observed. These anomalies have not been identified with auroral effects on a one-on-one basis, but do appear to be an attempt by the NUWAV program algorithms to handle changing auroral morphology within one data interval.

All of the spatial PSD's observed during this interval exhibit average power law behavior, both for N-S and E-W coordinates. The power law behavior ranges over the spatial frequency range 0.01 to about 1 km^{-1}. PSD's in the E-W coordinate appear to be more erratic and some extend in power to below 0.001 Km^{-1}. This pattern is quite consistent with the usual alignment of auroral arcs in the E-W direction, thus producing a very low spatial frequency component in their PSD's.

With the exception of the anomalous effects noted above, all PSD spectral indices are approximately $k^{-1.3}$. Averages over all PSD's show that the N-S spectral index is -1.3 ± 0.4 and the E-W spectral index is -1.15 ± 0.3. From the standpoint of the appearance of the diffuse auroras after discrete forms and breakups have disappeared, it is not unexpected that the precipitating patches would be more or less uniform in the N-S and E-W directions. Unfortunately because of the long integration time of the ASC photographs and their relative insensitivity, it is not possible to confirm this observation by

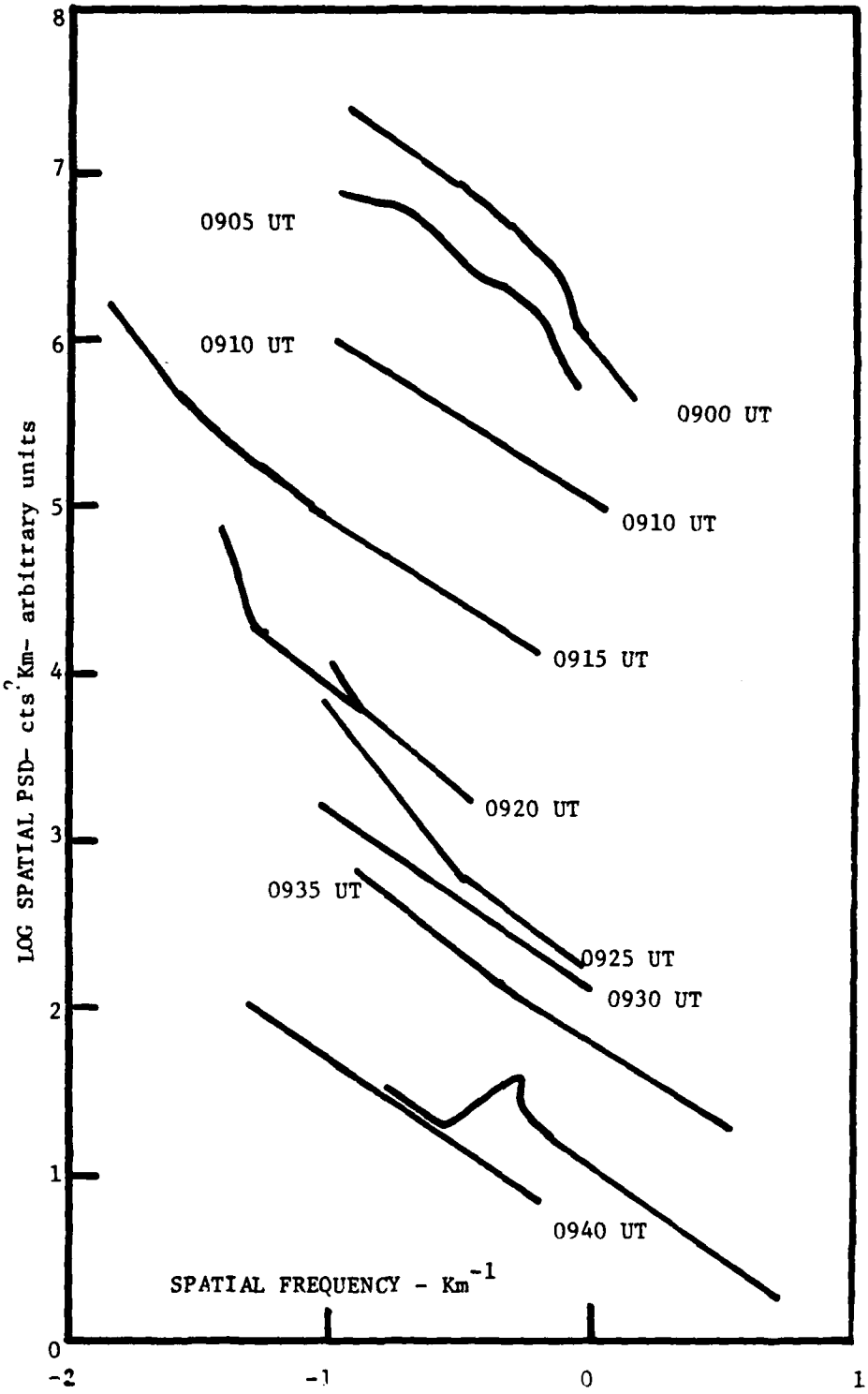

Figure 16 Spatial PSD's for the interval 0900 to 0945, 16 February, 1980, computed by the NUWAV code for the E-W direction.

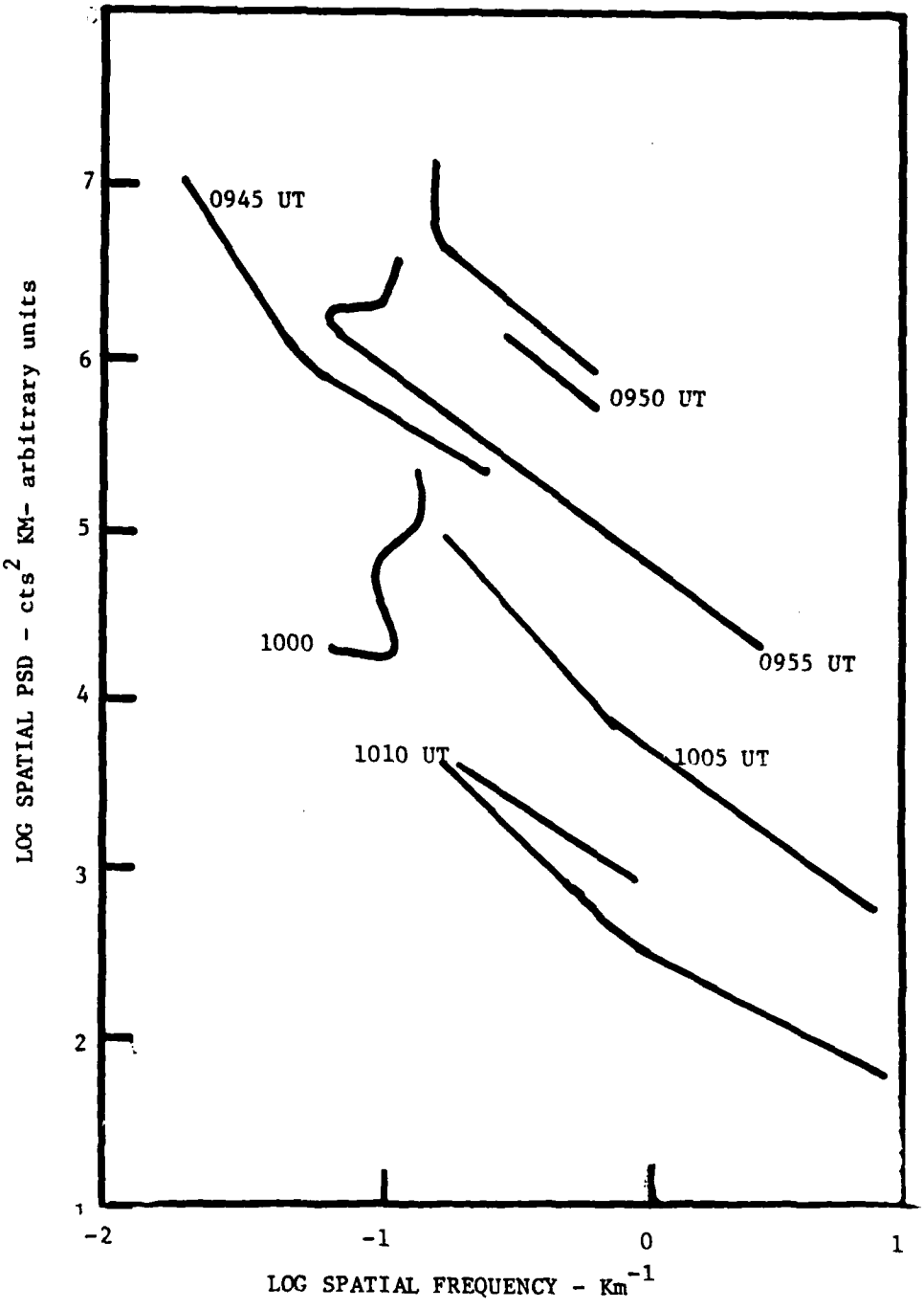

Figure 17 Spatial PSD's for the period 0950 to 1010 UT; continuation of figure 16 NUWAV computation for E-W coordinates.

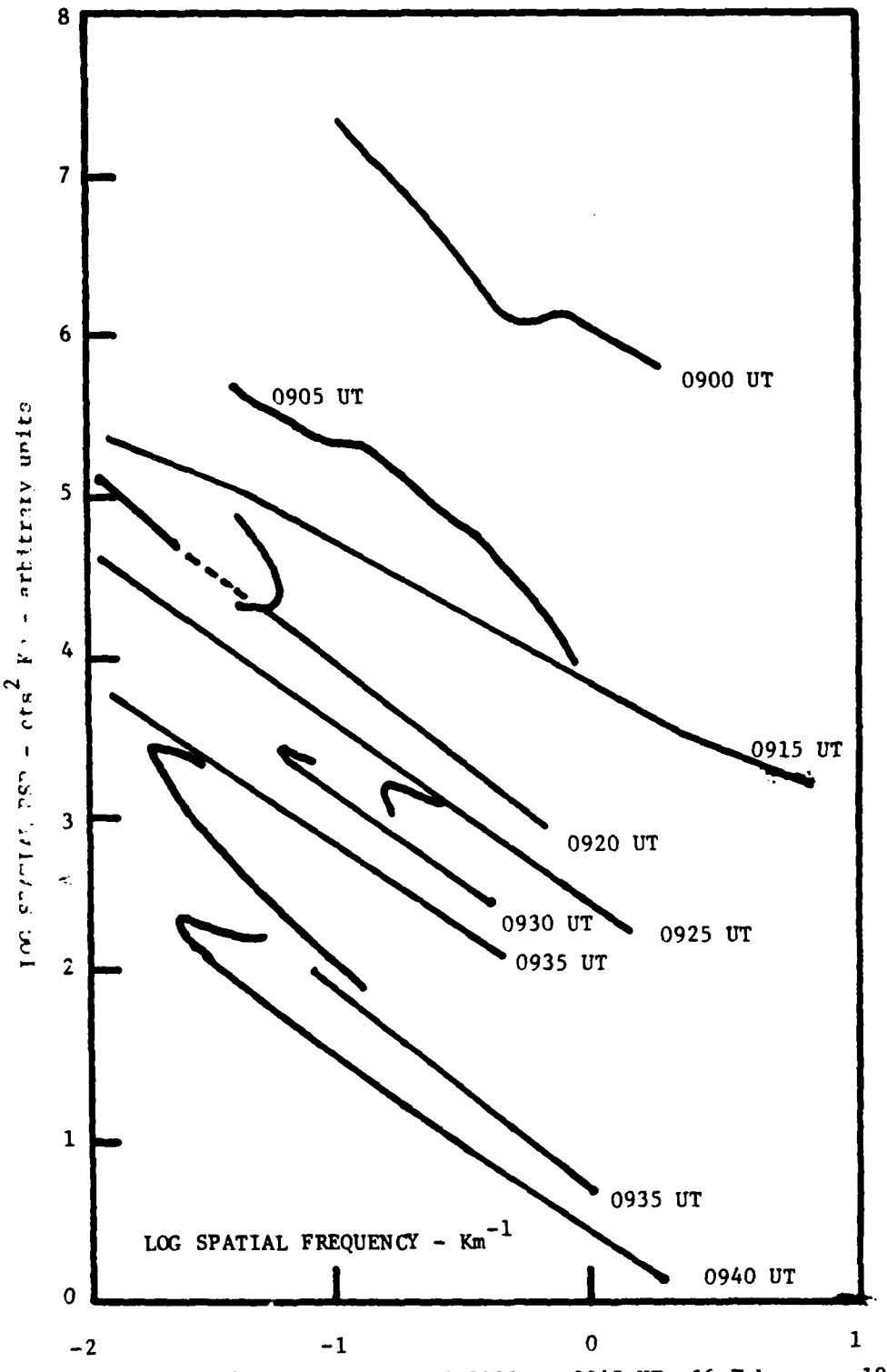

Figure 18 Spatial PSD's for the period 0900 to 0945 UT, 16 February, 1980. Computed by the NUWAV code for N-S coordinates.

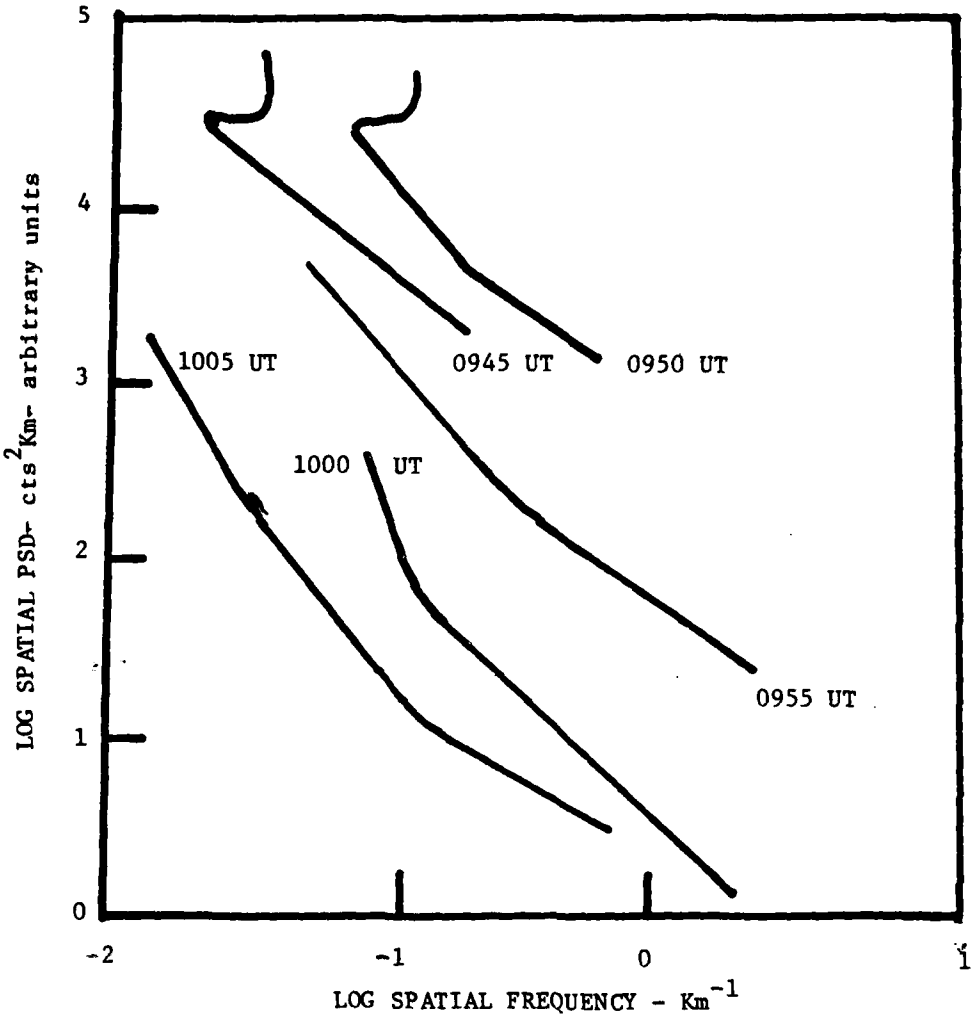

Figure 19 Spatial PSD's for the period 0950 to 1010 UT, continued from figure 18. NUWAV computation for N-S coordinates.

an independent technique.

It may be concluded on the basis of these and other observations of spatial PSD's during and after auroral breakup and poleward surge that the horizontal emission structure is relative isotropic with respect to intensity fluctuations. This conclusion may not be generalized to other forms such as quiet arcs, N-S aligned bands, or other highly structured forms such as omega loops, etc.

2.5 Applications of Auroral Structure Measurements

Temporal and spatial PSD's of auroral spectral emission irregularities have been measured over the spatial scale of 0.001 to 1 km^{-1} and the temporal scale of 0.01 to 0.5 Hz concurrently. The measured emission structure directly reflects the spatial and temporal characteristics of the auroral precipitation as it deposits energy into the atmosphere. Energy deposit with concurrent optical state excitation and ionization in the atmosphere impacts a number of defense related systems. Measurements of spatial and temporal structure presented herein, plus logical extensions to this data base, are directly relevant to characterizing the temporal behavior of visible, near IR, and IR radiance in several bands observed by staring sensors. Spatial structure exhibited herein, plus logical extensions of the k-space range of the PSD measurements also contribute directly to the data base relating to optical emission observed by both staring and scanning sensors. Finally, both temporal and spatial variations in atmospheric energy deposit, whether by natural or artificial phenomena also affect the distribution of ionization in the ionoshere with consequent effects to electromagnetic communications and radar systems.

Transfer of ground-based optical measurements of auroral irregularities in the temporal and spatial domains has already been initiated by Kumer (reference 12) for several IR bands of interest to the systems community. However, in order to provide a more comprehensive data base for systems use, continued effort to define spatial and temporal PSD behavior under a greater variety of auroral conditions is required. Much of the ground-based spectrophotometric data is already available and merely requires processing.

3. COORDINATED EXPERIMENTS

3.1 Experiment Summary

A coordinated experimental program was undertaken at the Chatanika optics research site as was outlined in section 1.3. As an alternative to coordination with aircraft and rocket experiments, coordinated measurements were made with the Chatanika incoherent scatter radar in collaboration with SRI International personnel.

Coordinated measurements were conducted during two observing periods, February 1979 and February 1980. Synposes of the optical data obtained during these periods is contained in Appendix A to this report.

The goals of the coordinated radar-optical experiment were as follows:

- o Improve and continue the cross calibration of ionospheric and auroral parameters which are measured by each technique.
- o Extend the range of coordinated optical and radar measurements such that the mutual capabilities of these instruments can be evaluated and extended to auroral intensities approaching certain nuclear burst phenomena's effects upon the ionosphere.
- o Evaluate the potential of the spectrophotometric measurements for providing important auroral and ionospheric measurements in support of DNA/AFGL infrared and ionospheric experiments at Poker Flat Alaska after the incoherent scatter radar is moved, eg. after about 1 March, 1982.

As a result of the coordinated optical-radar observations, two auroral phenomenological regimes were chosen for study: a period of intense pulsating aurora, and a post breakup period during which fairly intense, but low energy bands were observed. The rationale for this choice was as follows: intense pulsating aurora (periods up to several seconds) tests the analytical procedure for modeling the ionospheric response to transient phenomena such electron injection events. In this case, models cover both the atmospheric radiance emission in the visible and IR bands and the electron density change.

The mean energy parameter for pulsating auroras is fairly large, eg., the average precipitating electron energy is about 10 kev or so. A contrasting picture is presented by the post breakup events which have low mean energy, but which still present significant energy deposit and optical intensity. Comparison of these two events allows prediction of IR excitation efficiency in several bands over an altitude range of approximately 90 to over 140 km. These two events were particularly valuable in that the range of the HAES program modeling capabilities was extended.

3.2 Instrumentation

The principal spectrophotometric instrumentation used for the coordinated experiments were the Meridional Scanning Photometer (MSP) and its associated control and data system. This instrument was bore-sighted with the Chatanika radar at geomagnetic zenith. The Chatanika incoherent scatter radar is described in detail in reference 14 and was operated by the SRI International field crew for these experiments. Instrumentation parameters pertinant to the coordinated experiments are described in Table 7.

Table 7

COORDINATED EXPERIMENT INSTRUMENTATION PARAMETERS

PARAMETER	RADAR	PHOTOMETER
Field of view	0.6^{o}	3^{o}
Horizontal Resolution (at 110 km)	1.1 km	5.5 km
Integration Time	1 sec.	1 sec.
Vertical Resolution	1.5 km (range gate)	Integrated through layer
Orientation	Geomagnetic Zenith 219^{o}Az, 76.5 El.	Geomagnetic Zenith

3.3 Data Analysis

Incoherent scatter radar and optical measurements are reduced and analysed independently at SRI International and at LMSC respectively. After processing the individual data series, comparisons of equivalent quantities, eg., total energy deposit in the atmosphere, the mean energy parameter, electron density vs. altitude, etc. are carried out using a common time basis.

Analytical routines used to process the incoherent scatter radar data have been extensively reported by the SRI group (see for example, references 15 and 16). In this report, the results of the radar analysis conducted by SRI International are compared with equivalent data obtained from analysis of the spectrophotometric data.

3.3.1 Analytical Basis for the Spectrophotometric Data Analysis

An extensive literature exists relevant to the spectrophotometric intensities and occurrence statistics for many types of auroras (ref. 17 & 18). In addition, analytical models have been constructed by a number of workers which relate the specific spectral emission intensities to parameterized descriptions of the precipitating particle flux. For example, the spectral intensities of the H_α and H_β emissions at 656.3 and 486.1 nm. respectively may be related to the flux of precipitating protons (ref. 19). The total energy deposited in the atmosphere by the precipitating particle flux is determinable from the intensity of one or more of the N_2^+ 1st Negative Bands because of their well known fluorescence efficiencies. Finally, an estimate of the mean energy parameter for a quasi-Maxwellian precipitating electron flux may be determined by measurement of spectrophotometric ratios of the $OI(^1D-^3P)$ and $OI(^1S-^1D)$ transitions at 630. and 557.7 nm respectively to the intensity of one of the N_2^+ 1st Negative bands.

Spectrophotometric analyses presented in this report are based upon a simplified analytical version of the model developed by Rees and Luckey (ref. 20). The characteristics of this model are summarized in Table 8. It should be noted that for practical purposes, emissions caused by precipitating protons are not included because these effects are usually small in

the post-midnight sector. Previous observations of H_γ emission intensity at 486.1 nm. tends to confirm this approximation, although it is recognized that this would not be the case in the pre-midnight proton arc region where proton and electron fluxes may be approximately equal.

TABLE 8

SPECTROPHOTOMETER ANALYSIS MODEL

Electron Energy Distribution	Maxwellian ($E=j_o E \exp(-E/\mathcal{E})$)
Distribution Model Parameters	Total Energy ($E_t = j(E)\, dE$
	Mean Energy, $\mathcal{E}$
Derivation of Total Energy	$E_t = K\, I(427.8\ nm\ band)$
Fluorescence Efficiency	$K = 210$ Rayleighs $erg^{-1}cm^2$ s.
Mean Energy Parameter	$R_1 = I(630.\ nm)/I(427.8\ nm)$
	$R_2 = I(557.7\ nm)/I(427.8\ nm.)$
	$= A_i R_i^{-n_i}$
	where, $A_1 = 1.4$ $n_1 = 0.67$
	and $A_2 = 20$ $n_2 = 1.82$

The Rees and Luckey model has been simplified in two ways. A constant N_2^+ 1st Negative band fluorescence efficiency was adopted because previous measurements (ref. 21) showed that the cited variation in value (160 to 220 Rayleighs $erg^{-1}cm^2$ sec.) was experimentally measureable for mean energies below only about 1 kev, hence was not really observable in the data for more energetic auroral forms. The higher, and constant value was adopted on this premise. The second approximation involves the slight dependence of the spectrophotometric ratios R_1 and R_2 upon the total energy flux. Again, this dependence was not experimentally observable, therefore it was not included in the analytical model used herein. The simplified analytical relationship between spectrophotometric ratios and the mean energy parameter used in this analysis is illustrated in figure 20. The slight degree of energy dependence of the mean energy parameter as measured by the ratio R_1 is illustrated by the horizontal bars. These bars represent a change in total energy of a factor of 10, or a total range of I427.8) from 0.3 to 3 kR.

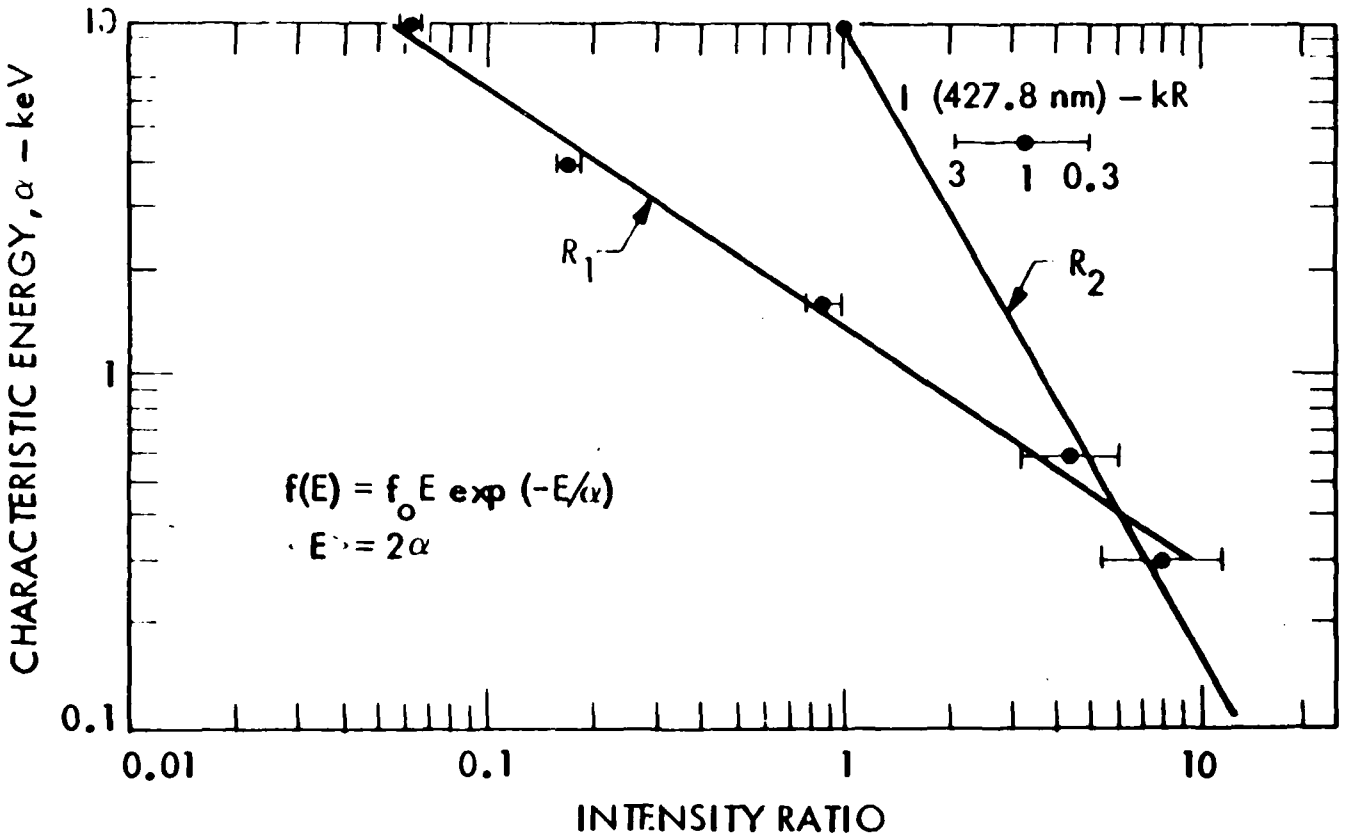

Figure 20 Simplified analytical model of the dependence of the characteristic energy (mean energy parameter), α, upon spectrophotometric ratios.

3.3.2 Derivation of Ionospheric Quantities from Spectrophotometric Data

Auroral precipitation produces ionization in the D- and E-regions of the ionosphere, depending upon the total energy deposited and the characteristic mean energy of the precipitating flux. For many conditions of auroral precipitation, it is reasonable to assume that a quasi-equilibrium condition exists in the ionosphere such that the following conditions hold for local time variations of electron density in a given volume: $dN_e/dt = Q - \alpha(\text{eff}) N_e^2$. Q is the ion pair production rate, α(eff) is the effective electron-ion recombination coefficient and N_e is the measured electron density. If transport of ionization is neglected and the temporal behavior of Q is not impulsive compared with the recombination time, then the term dN_e/dt approximates zero and the electron density at a given altitude may be related directly to the ion pair production rate, Q. Spectrophotometric measurements provide a direct evaluation of the height integral of Q because the ion pair production efficiency (35 ev/ion pair) is proportional to the energy deposit per unit volume as well as to the N_2^+ fluorescence efficiency. The altitude profile for energy deposit per unit volume may be derived from the mean energy pameter of the precipitating electron flux, hence two quantities may be derived from spectrophotometric data that are directly comparable to the radar measurements: Total energy deposit, E_t, and electron density vs. altitude, $N_e(z)$. Simultaneous measurements of these quantities by photometric and radar techniques allows derivation of the altitude profile of the effective recombination coefficient α (eff). This experiment, in fact, was carried out and reported by Wickwar et al (ref. 21) using simultaneous photometric and radar measurements. The altitude model for the effective recombination coefficient used in this analysis is derived from the Wickwar model (ref. 22).

Electron density vs. altitude is modeled using the SRI TANGLE code. This code uses the input parameters E_t and which are derived from spectrophotometric data and computes $N_e(z)$ following the energy deposit model of Burger and Seltzer (ref. 23) and is similar to codes developed by Rees (ref. 24 and the AURORA Code developed at LMSC (ref. 25). The TANGLE code has been compared with other energy deposit and ion pair production rate codes and has been shown to accurately represent the ion pair production rate vs. altitude

throughout the auroral E-region. An example of the computation of $N_e(z)$ for an intense aurora is illustrated in figure 21. Comparisons between TANGLE computations based upon spectrophotometric data input and the radar measurements of $N_e(z)$ are presented in the next section.

3.4 COORDINATED MEASUREMENTS OF AURORAL CHARACTERISTICS

Two sets of coordinated radar and photometric measurements are reported. Observations of an intense pulsating aurora were made on 3 March, 1978, and an intense polar cap auroral display was observed on 16 February 1980. During both experiments, the radar and photometer fields of view were boresighted at geomagnetic zenith and the data were obtained over identical time periods with comparable integration times.

3.4.1 Pulsating Aurora Experiment

3.4.1.1 Experiment Goal

The goal of the pulsating aurora experiment was to investigate the ability of the spectrophotometric measurement technique to monitor the total energy deposit, the mean energy parameter of the precipitating electrons, and to characterize the electron density profile under conditions of pulsating aurora wherein the strict conditions of ionospheric equilibrium would not be met. These measurements were verified by comparison to incoherent scatter radar measurements of electron density profile.

Previous measurements on weaker pulsating auroras made by Wickwar et al (ref. 21) and by Vondrak and Sears (ref 26) indicated that quantitative agreement between the two experimental techniques could be achieved under the quasi-equilibration approximation. During the coordinated measurements on March 3, 1978, the range of agreement was extended to much more intense and more energetic pulsations.

3.4.1.2 Optical and Radar Measurements

The measurements were undertaken during a period of very intense pulsating auroras during the morning period of 3 March, 1978(1250-1350 UT). A short period of particularly intense and rapid pulsations was chosen for a

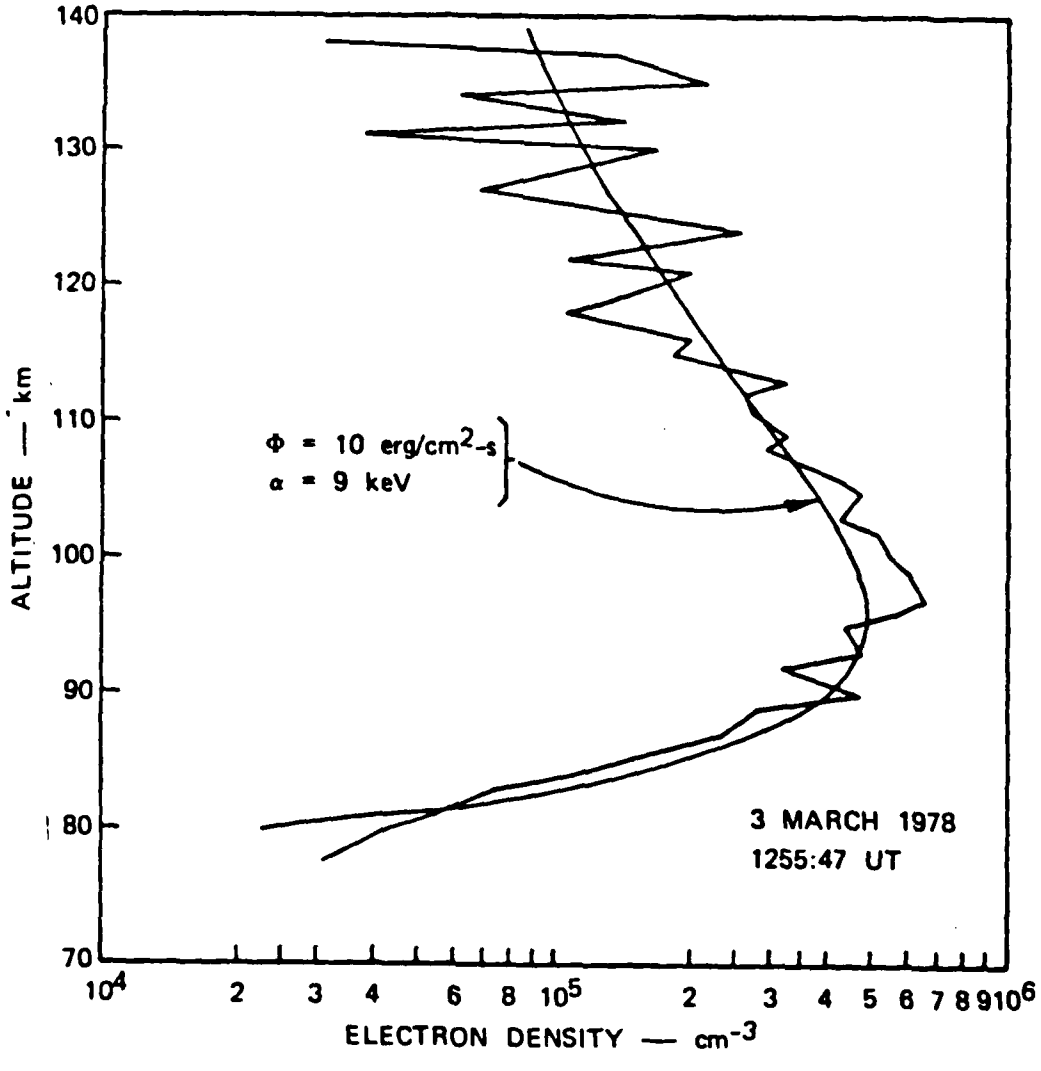

Figure 21 Electron density vs. altitude computed using the TANGLE code with spectrophotometric data input compared with an N_e profile measured with the incoherent scatter radar.

detailed analysis and comparison of radar and photometric data. This segment shows more intense precipitation than other data during the observing period, but is not unique otherwise.

Spectrophotometric intensity measurements of 427.8, 557.7, and 630. nm emissions are illustrated in figure 22. The dynamical nature of the pulsations is clearly evident in the two shorter wavelength emission which have short radiative lifetimes. The high mean altitude of emission and longer lifetime of the OI (^{1}D) state (630. nm) effectively damp out fluctuation amplitudes in this emission feature.

Using the analytical approach described in section 3.3, the total energy deposited in the atmosphere as well as the mean energy parameter of the precipitating electron flux is plotted in figure 23. The relative modulation of the pulsation energy is approximately 30 percent about the mean value. The average pulsation duration is about 3.2 sec. and the average interpulse period is about 7.6 sec.

Previous measurements of the total energy deposit and the mean energy parameter in pulsating auroras indicated that the pulsations were a result of a modulation of the mean energy parameter, rather than a modulation of the total electron flux (see for example references 27 and 28). In order to determine whether the observed pulsating aurora followed this behavior pattern, the number flux of precipitating electrons during the pulsations was computed from the following expressions:

$$F(\text{electrons cm}^{-2}\text{s}^{-1}) = E_t/(2\alpha e),$$

where the energy per electron is $e = 1.6 \times 10^{-9}$ erg kev^{-1}, and α is the mean energy parameter for a quasi-Maxwellian distribution.

Figure 24 illustrates the result of this computation for a short data period. The average precipitating electron number flux is 7.2×10^8 el cm^{-2}sec^{-1} with a standard deviation of about 13 percent. The fact that this value for precipitating electron flux appears to be common to several classes of pulsating auroras is discussed in more detail in reference 28.

Incoherent scatter radar measurements were made of the electron density vs. altitude through the observing period. For purposes of illustration, two highly contrasting pulsation observations are chosen; a large positive pulsation and a minimum between pulsations. Figure 25 illustrates the electron

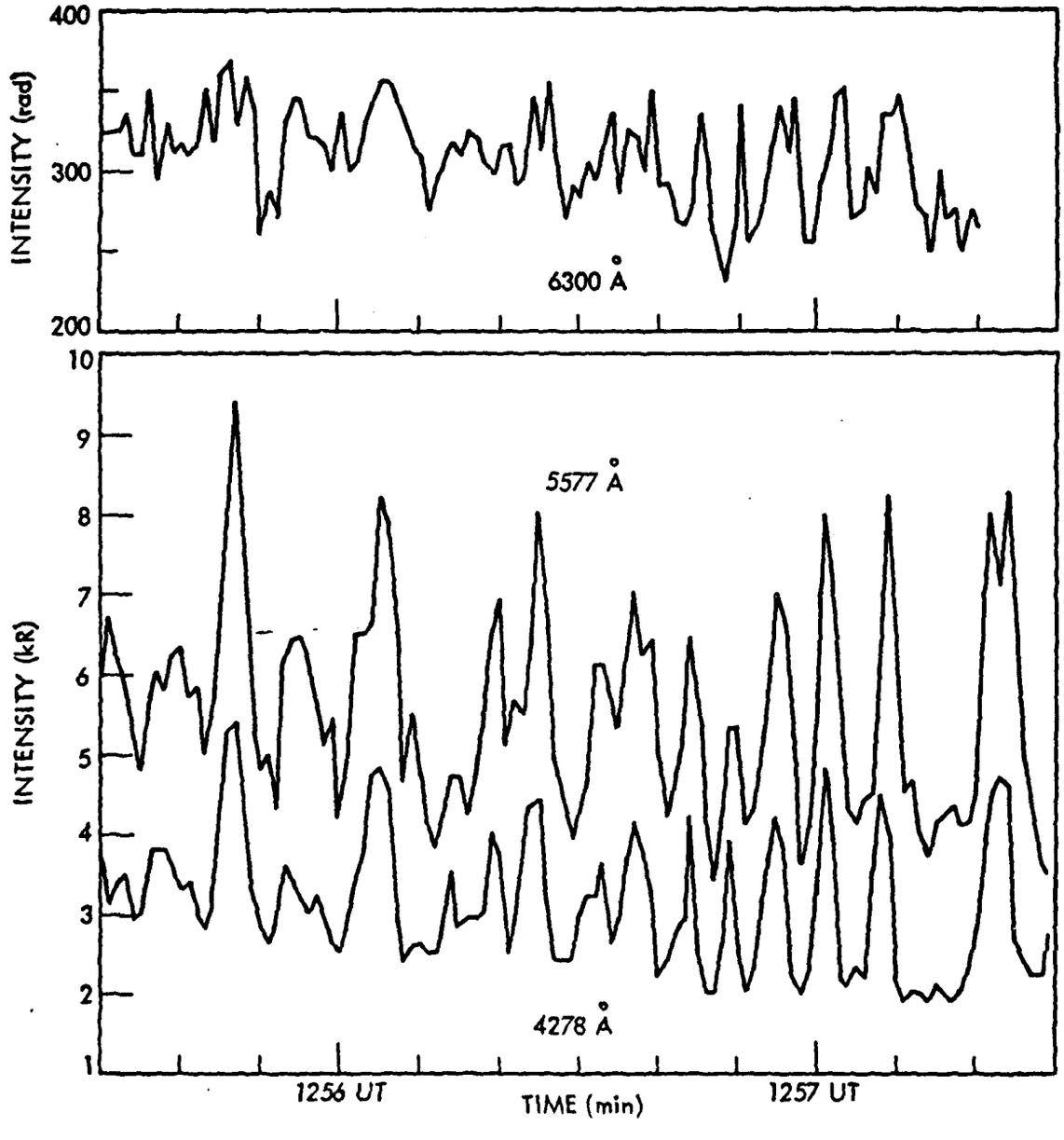

Figure 22 Spectrophotometric measurements made during an intense pulsating aurora. Observing period; 3 March, 1978.

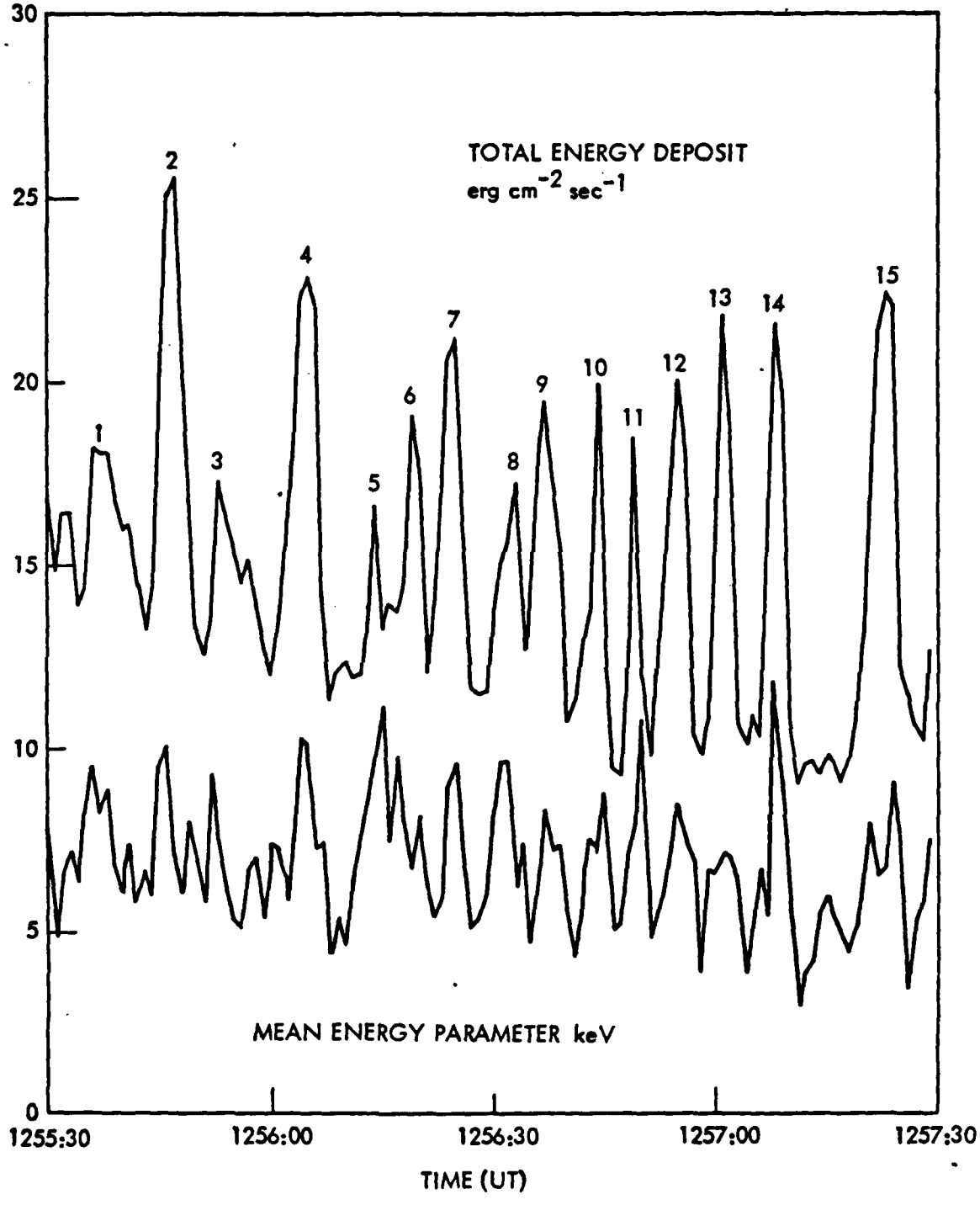

Figure 23 Total energy deposited in the atmosphere during the intense pulsating aurora illustrated in figure 22 and the mean energy parameter.

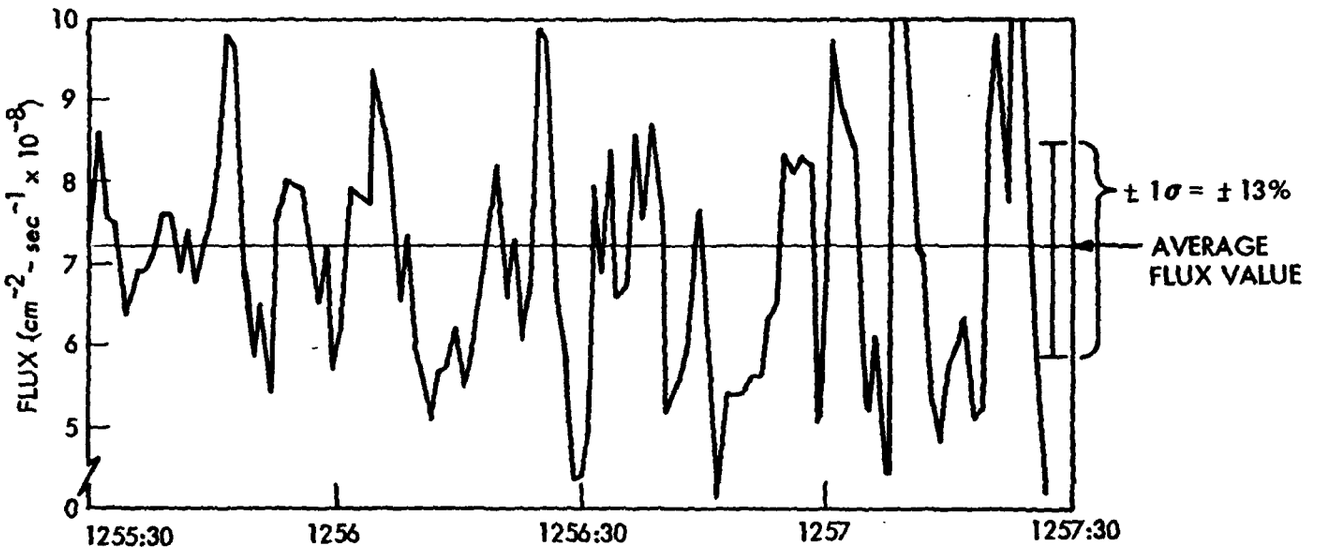

Figure 24 Precipitating electron flux variation during the pulsating aurora illustrated in figures 22 and 23. A *quasi*-Maxwellian electron energy distribution is assumed.

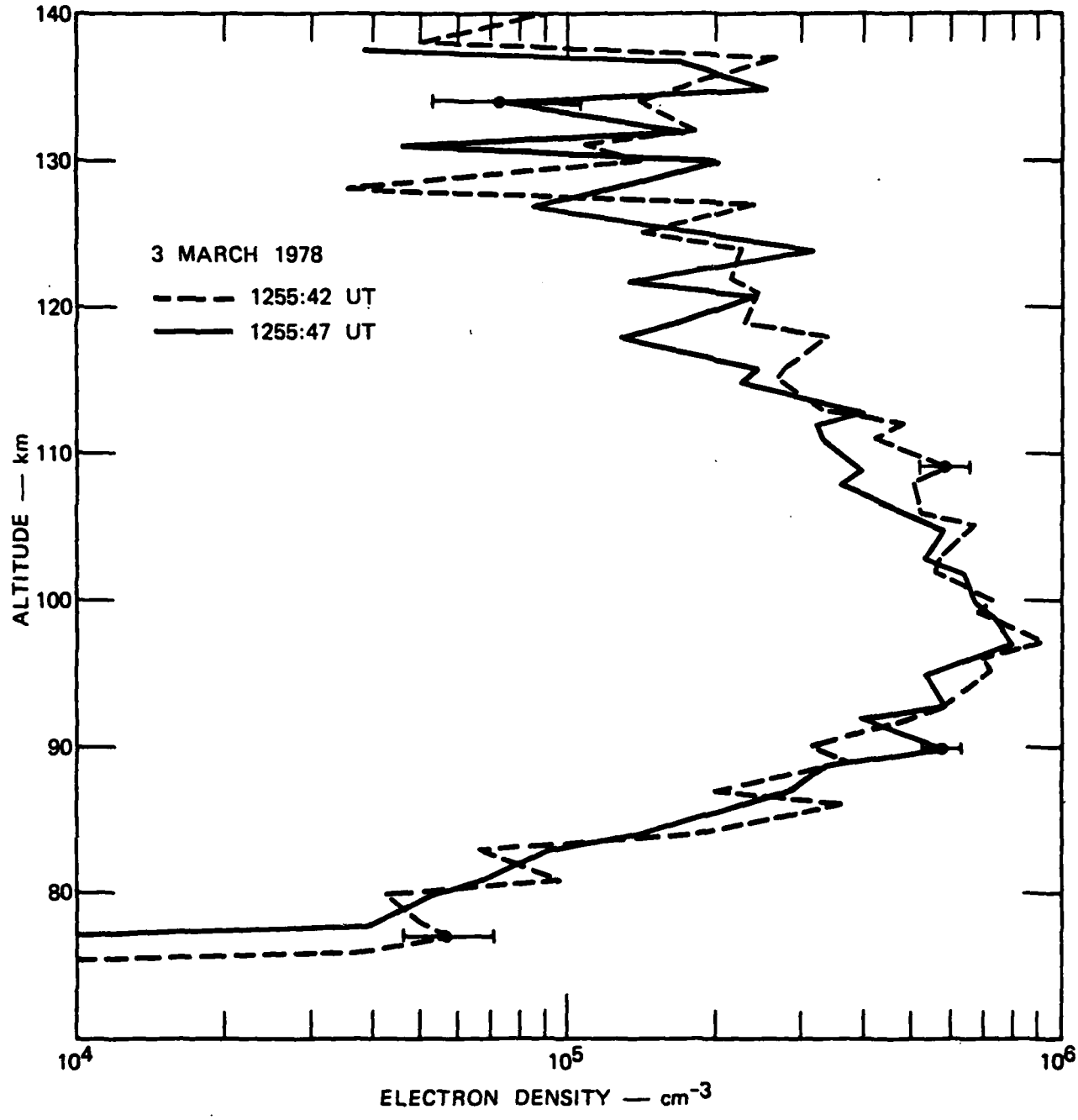

Figure 25 Incoherent scatter radar measurements of electron density vs. altitude made during a pulsation peak (#2, figure 23) and during a minimum (2-3, figure 23).

density vs. altitude measured by the incoherent scatter radar for these two times. The noteworthy feature of this data plot is that there is no significant difference between the pulsation maximum and minimum electron density profiles even though the amplitude of the pulsation total energy deposit is at least twice that of the interpulse minimum condition. These examples were selected for pulse number 2 (1255:42) and the interpulse period,2-3 at 1255:47 UT.

3.4.1.3 Analysis of Optical and Radar Data

In order to explain the apparent lack of response of the ionospheric electron density profiles to pulsation-induced ionization disturbances, it is necessary to consider the ionospheric electron density profiles which would be predicted using the TANGLE code and the spectrophotometric input parameters vs. the responsivity of the ionosphere to impulsive types of ion pair production rate sources. The measured electron density vs. altitude is compared with predictions of the same quantity for pulsating maximum and minimum conditions using the TANGLE code in figure 26. Here, it is apparant that the shape of the $N_e(z)$ curve is determined by the higher energy precipitation during pulsation maximum whereas the total magnitude of the electron density is closely related to some total energy deposit value between pulsation maximum and minimum.

Reference to the quasi-equilibrium ionization model shows that the total modulation in electron density, given a source transient with very long duration compared with the equilibration time would be approximately 40 percent ($\sqrt{2}$) for a transient amplitude double that of the previous value. Ionospheric equilibration time for this case may be defined (see ref. 27) as $\tau = 1/2\alpha(\text{eff})\, N_e$. Therefore, to a first approximation, the fractional increase in electron density at a given altitude is $F = 3.2/\tau$, where the value 3.2 comes from the average pulsation duration.

For the case of the intense pulsating aurora described herein, the radar data were smoothed to approximate the shape of the photometrically-derived $N_e(z)$ curve and the ionospheric equilibration time was computed over the altitude range pertinant to the auroral E-region. The ionospheric relaxation or equilibration time vs. altitude for these conditions is illustrated in figure 27.

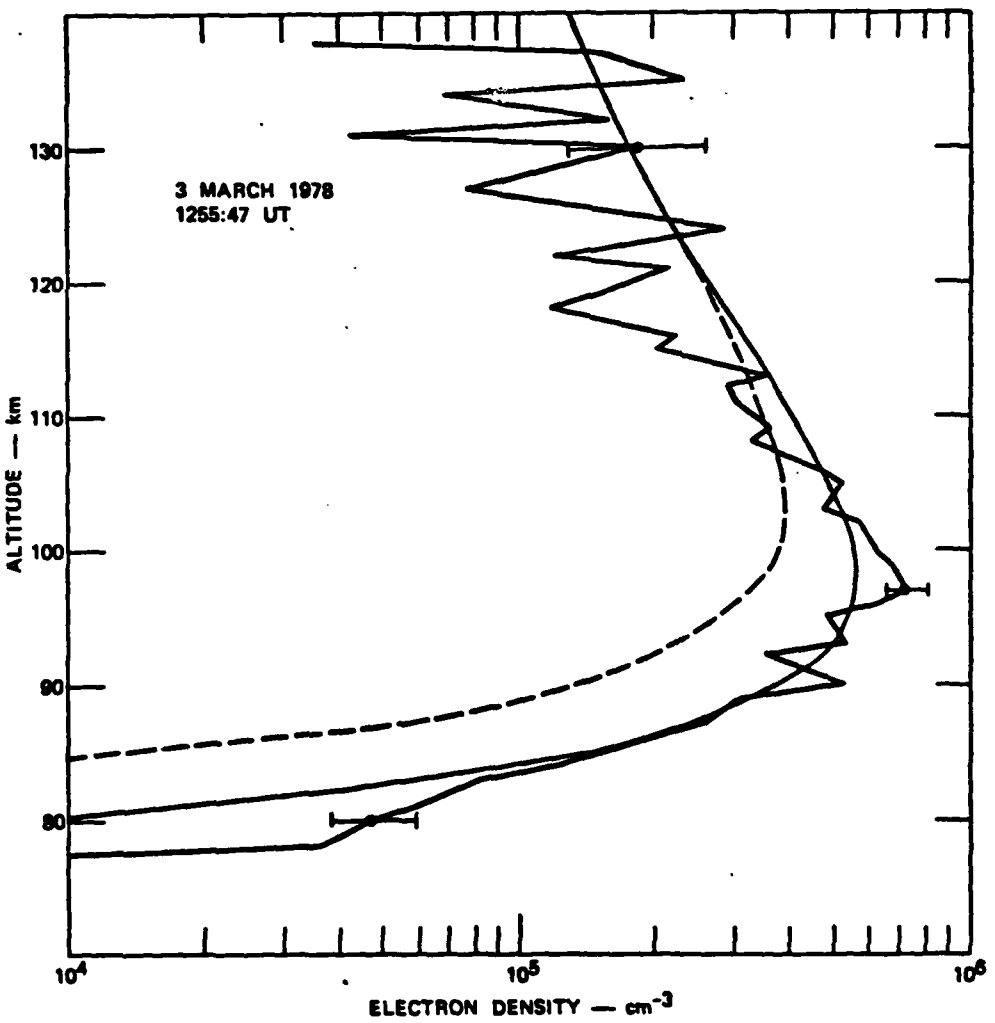

Figure 26 Comparison of electron density vs. altitude with TANGLE code predictions for pulsation maximum and minimum conditions.

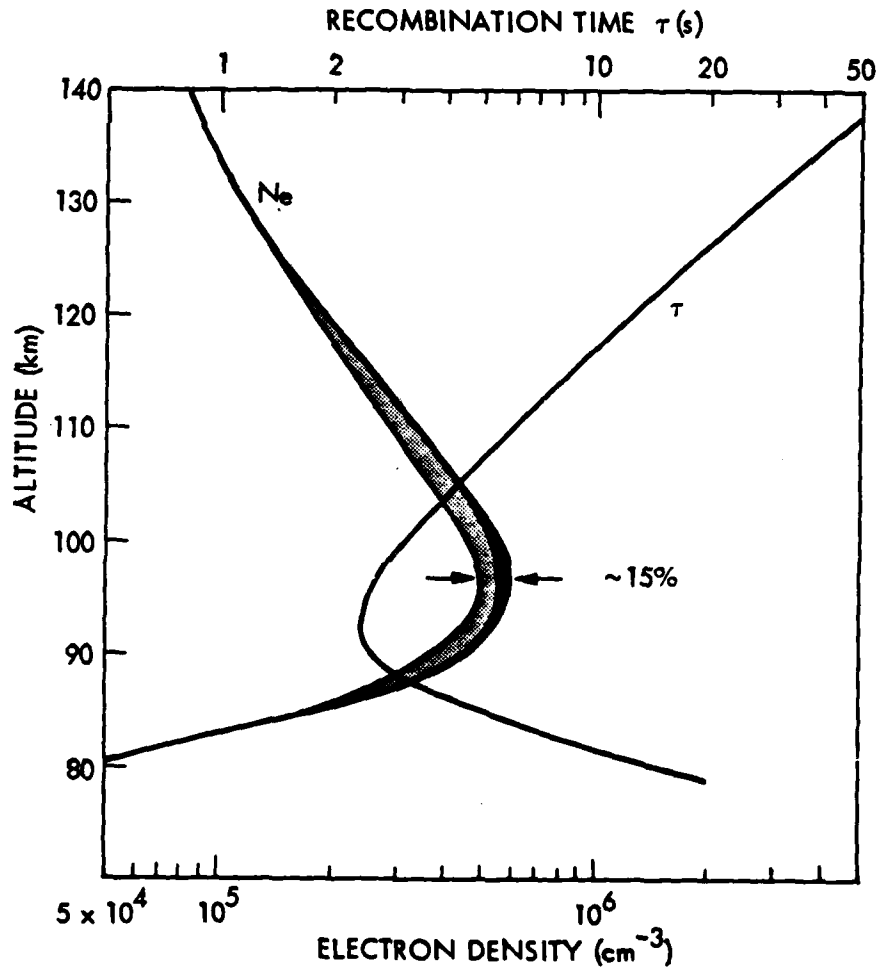

Figure 27 Ionospheric equilibration time vs. altitude for a typical electron density profile. The predicted range of N_e modulation during pulsations is illustrated by the shaded region.

Figure 27 also displays the electron density model used in the computation and the expected modulation of the N_e profile due to the fluctuations in the precipitating electron flux. Based upon this model, the maximum expected electron density variations about the mean value was only about 15 percent. Because this was an exceptionally intense pulsating aurora, it may be concluded that the electron density vs. altitude during less intense pulsating auroras is less than this value. In fact, during this experiment and previous pulsating aurora experiments, no measureable electron density pulsations greater than the estimated experimental error have been observed.

The combined spectrophotometric and incoherent scatter radar measurements of auroral and ionospheric quantities may be extended to more complex derivation such as estimation of height-integrated Hall and Pederson conductivities, the maximum density in the E-region and the altitude of maximum electron density. These quantities were computed using the TANGLE, UNTANGLE, and associated analytical codes resident at the SRI International incoherent scatter radar facility. Results of these computations for the intense pulsating auroral period are illustrated in figure 28. The time dependence of the ionospheric quantities in figure 28 suggests that they are nearly uncorrelated with the detailed pulsation behavior of the incoming precipitating electron flux except for the gradual fall-off of the overall precipitation intensity. Error bars on the maximum electron density curve show that the fluctuations of N_e about its average value are less than a factor $\sqrt{2}$ in magnitude.

These coordinated radar and spectrophotometer measurements show that the recombination lag time for the ionospheric ionization response to transient-like disturbances must be accounted for when using spectrophotometric data to predict ionospheric electron density. In other words, we have defined at least one auroral phenomenology condition under which the full transient, time dependent continuity equations must be used to predict ionospheric N_e, as opposed to previously cited cases wherein weak, long period disturbances which were handled adequately by quasi-equilibrium formulations. As discussed in detail in reference 27, the recombination lag time of the ionosphere and associated parameters such as height-integrated conductivities suggest that the role of ionospheric feedback mechanisms in the generation of pulsations is minimal.

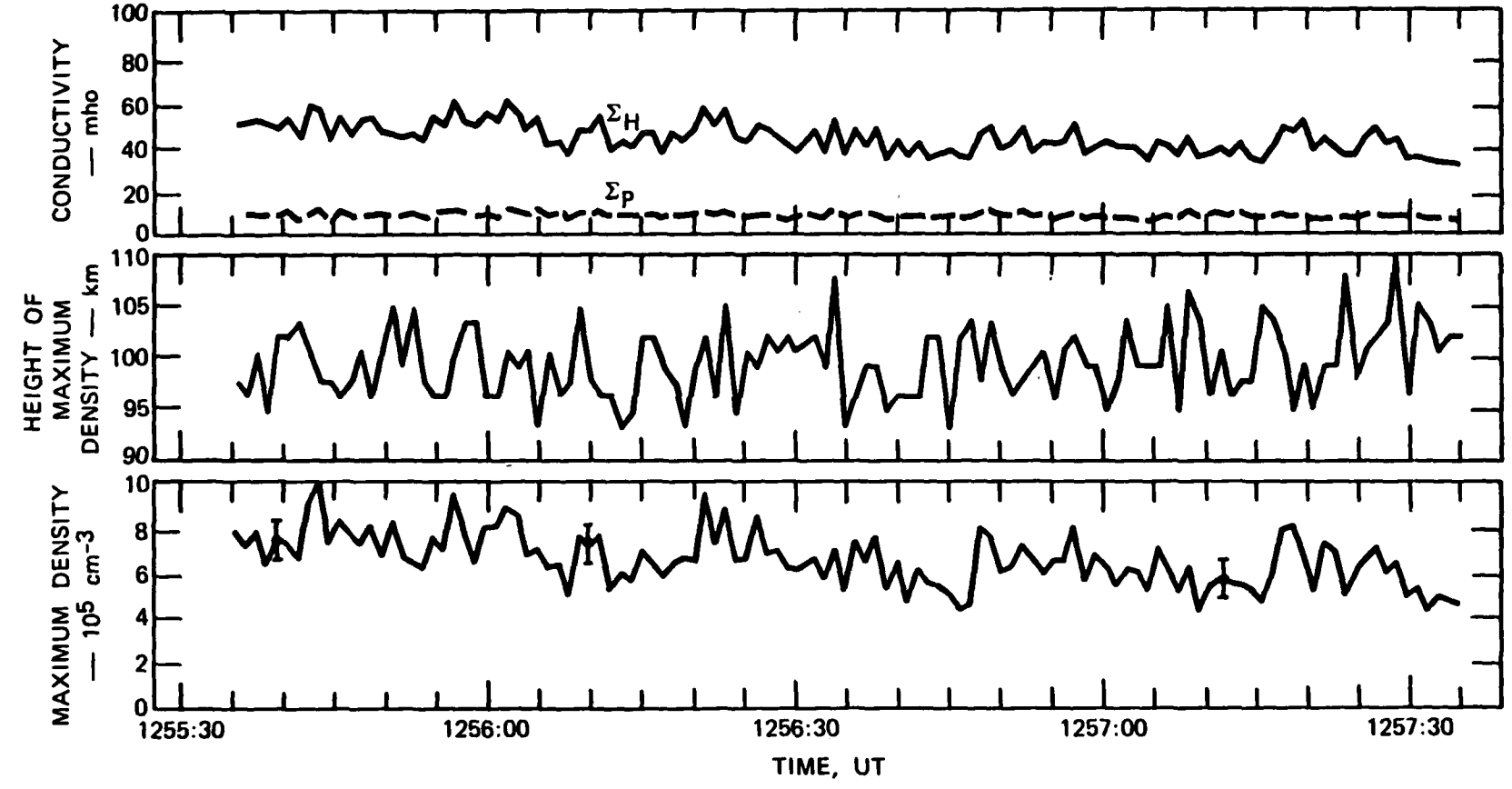

Figure 28 Time variation of ionospheric parameters during an intense pulsating aurora. All parameters illustrated are based upon incoherent scatter radar measurements of $N_e(z)$.

3.4.1.4 Conclusions: Pulsating Aurora Coordinated Experiment

Coordinated incoherent scatter radar and spectrophotometric measurements of intense pulsating aurora have shown the following results:

- o Measurements of total energy deposit and of the mean energy parameter for precipitating electrons during intense transient events must take into account the ionospheric recombination lag time if radar and spectrophotometric quantities are to agree.
- o Simultaneous radar and spectrophotometric measurements present a more detailed picture of the ionospheric response to auroral precipitation than either technique taken separately in that quantities such as ionospheric recombination coefficients and lag times can be evaluated independently.
- o During intense pulsating auroras, the nearly constant flux of precipitating electrons, and the nearly constant value for ionospheric electron density and conductivities implies that the pulsation mechanism is not strongly dependent upon ionospheric conditions. This conclusion has significant, but unevaluated, implications with respect to the rate and morphology of beta particle precipitation following a high altitude nuclear event.
- o The range of spectrophotometric observations of transient, pulsating precipitating particle events has been greatly extended as has the range of cross calibration with incoherent scatter radar measurement results. Spectrophotometric measurements of precipitating particle events may now be interpreted for total energy deposit up to about 25erg $cm^{-2}s^{-1}$ total energy deposit, mean energy parameter to 12 kev, and transient lifetimes down to approximately 3 seconds.

3.4.2 Coordinated Auroral Experiments: 16 February, 1980

3.4.2.1 Introduction

Coordinated radar and spectrophotometric observations were made during an intense auroral display on 16 February 1980. These observations were intended to extend the intensity and dynamical range of previous coordinated experiments, and especially to confirm the results of the analysis of the intense pulsating auroral experiment reported in section 3.4.1. Although a series of brief pulsations were observed between 0900 and 1130 UT, these were not remarkably different from previous observations. However, during the observing period, magnetic and auroral activity was extremely high, the auroral oval was located well to the south of the Chatanika observing site, and observations were made on a series of bands which appeared in the southwest and extended to the northeast. For most of the period of observations, this direction approximates a sun-aligned orientation. It is believed that the observed bands correspond to those observed on the poleward edge of the auroral region by the DMSP satellite. If this hypothesis is accurate, then the measurements described in this section constitute a unique coordinated data set on the poleward, sun-aligned auroral features.

3.4.2.2 Experimental Goals

Because experimental goals related to pulsating aurora could not be met during the analysis of this experiment, the opportunity to define the total energy deposit time history, mean energy parameter, and ionospheric response to the poleward auroral bands was taken.

3.4.2.3 Experimental Measurements

Four types of measurements were made for the 16 February, 1980 auroral experiment: spectrophotometric measurements of auroral intensities in the 427.8, 557.7, and 630. nm. spectral emissions; incoherent scatter radar measurements of electron density vs. altitude, using a very short pulse length and range gate in order to optimize vertical resolution; all sky camera photographs; and three beam photometer (3B1) measurements of auroral motion. The auroral motion data were used to develop the spatial and temporal PSD data presented in section 2. The radar data and all sky camera

were supplied through the courtesy of SRI International. Spectrophotometric instruments (MSP) and the incoherent scatter radar were bore-sighted at geomagnetic zenith for the duration of the experiment, 0900 to 1130 UT.

Previous sections have shown how total spectral intensities and their ratios may be used to infer the total energy deposit by precipitating electrons in the atmosphere, the mean energy parameter of the electron energy distribution, and the ionospheric response to the precipitating particle flux. An example of the spectrophotometric data used to infer these quantities is illustrated in figure 29. Analysis of these data in terms of E_t and $\mathcal{L}$ is illustrated in figure 30. Comparison of the total energy deposit, E_t, and the mean energy or hardness of the precipitating flux with detailed plots of peak electron density and the altitude of the density maximum measured by the incoherent scatter radar shows good qualitative agreement, eg., the altitude of electron density maximum decreases as the mean energy parameter increases, and the total electron density covaries as the total energy deposit. Because of the vast amount of data obtained during this observing period (approximately 8000 individual data sets of combined radar measurements of $N_e(z)$ and spectrophotometric measurements of emission intensities) a complete quantitative analysis of all data has not been attempted. The data presented for this experiment relates to the ionospheric response to the succession of auroral bands observed as compared with spectrophotometric measurements of the time variation of total energy deposit and the mean energy parameter for the precipitating electron flux.

The response of the ionosphere to the succession of auroral features previously described is illustrated in figure 31. This figure is keyed to the auroral all sky camera images displayed in figures 10 and 11. During the poleward expansion (panels A and B), the mean altitude of the E-region peak decreases from over 140 km to about 110 km. Furthur intensification of the aurora (panel C) shows a furthur decrease in the altitude of the ionized region as well as a significant increase in peak electron density from about 2×10^5 to over 1×10^6 el cm^{-3}. The dynamical nature of the poleward expansion is illustrated by both electron density measurements as well as by the spectrophotometric measurements.

The long term response of the ionosphere is comparable to the decay in

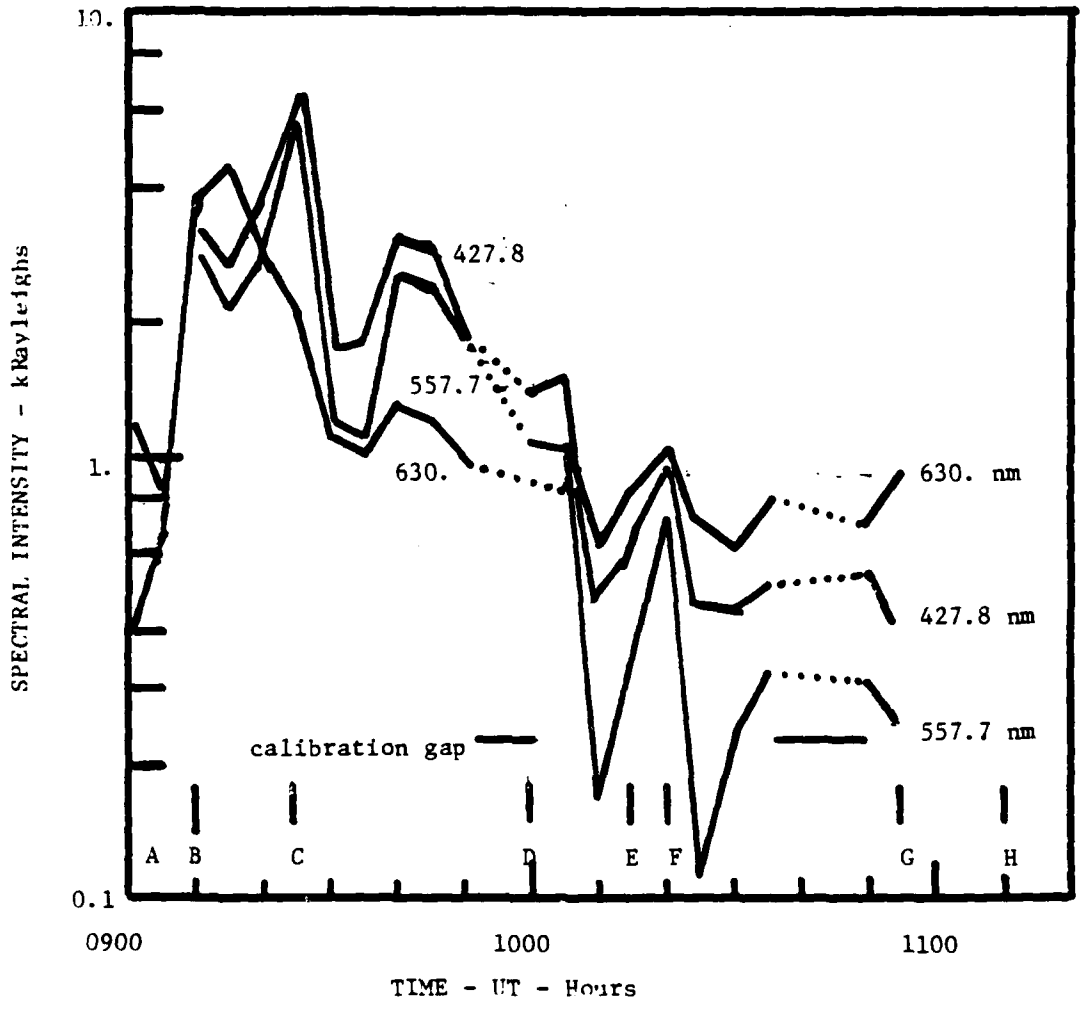

Figure 29 Spectrophotometric intensity measurements for the observing period 0900 to 1100 UT, 16 February, 1980. Data are plotted at five minute intervals.

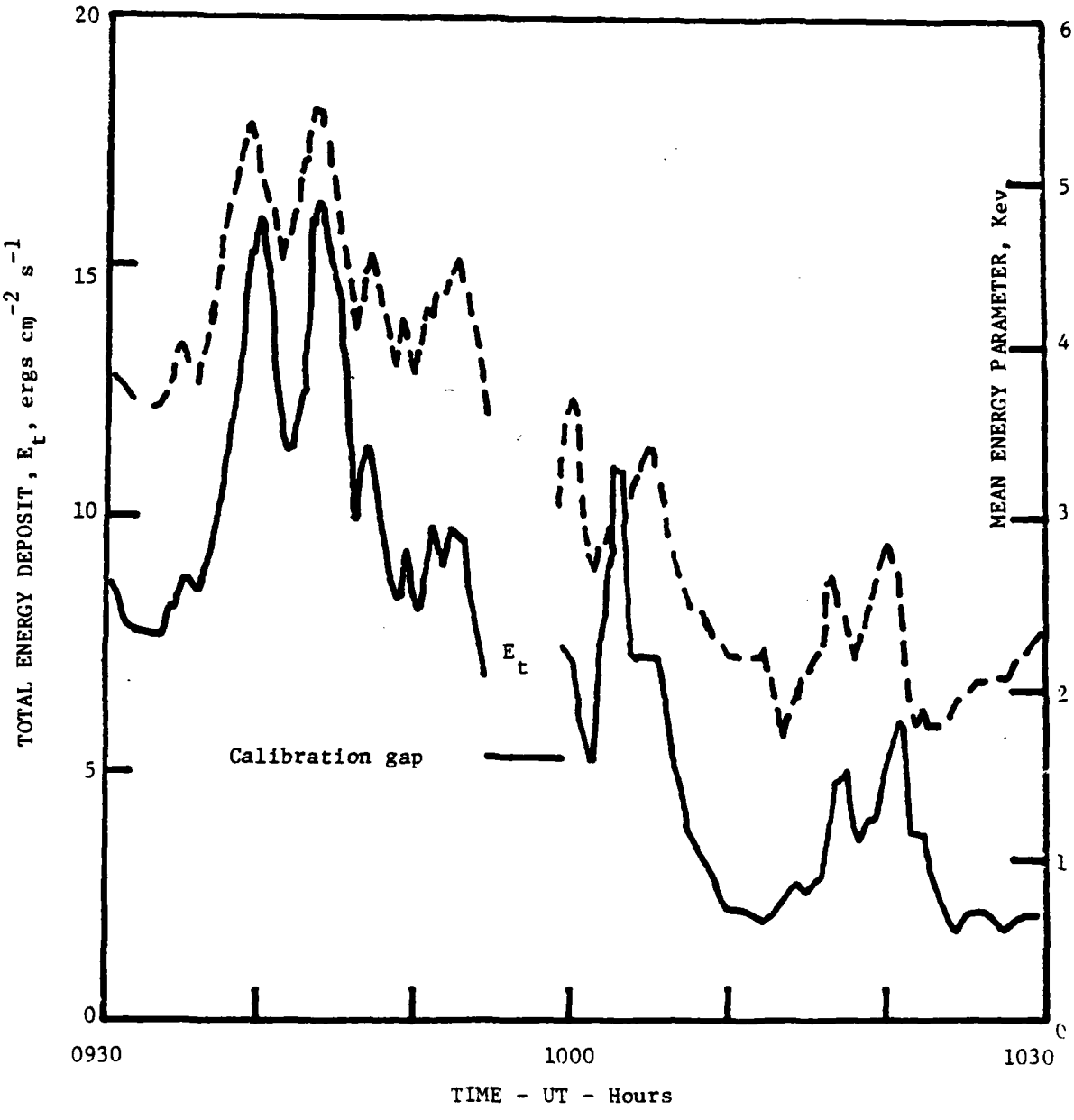

Figure 30 Total energy deposit and mean energy parameter for precipitating electrons during the 0930 to 1030 UT intervalselected from figure 29.

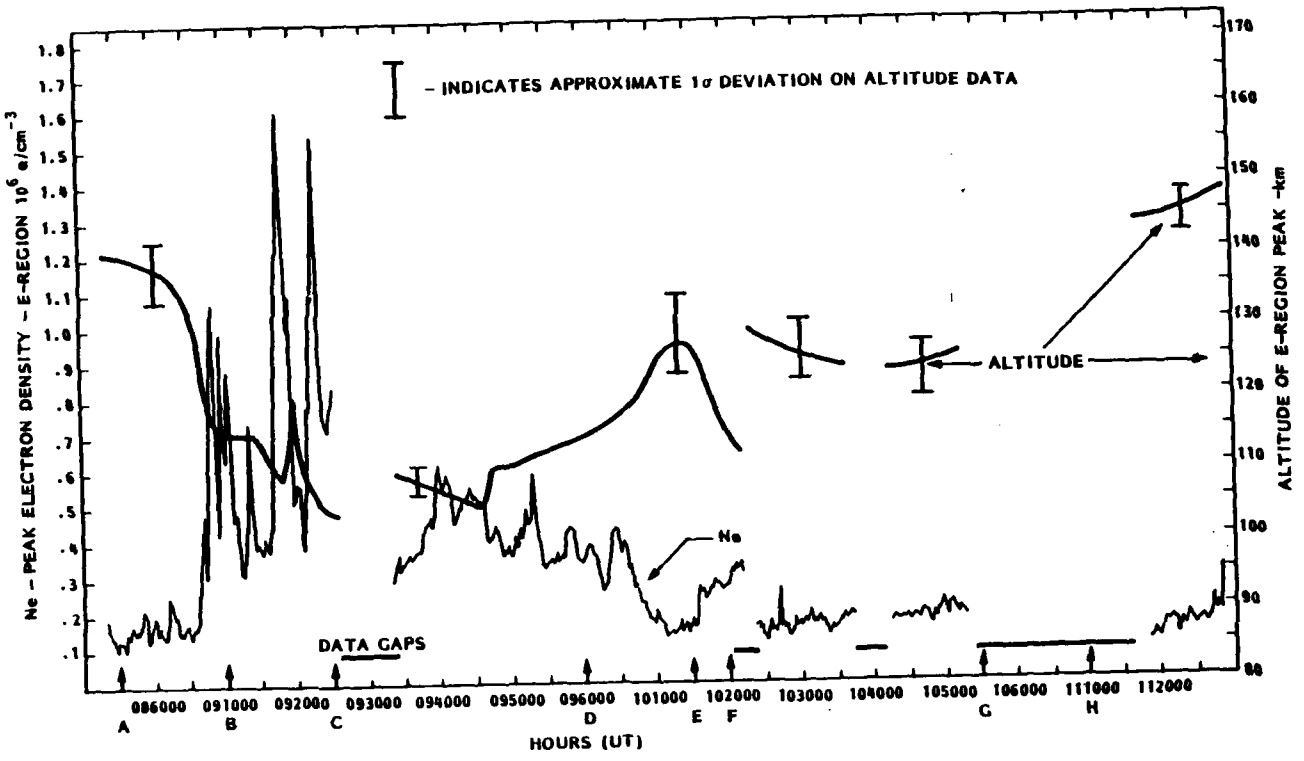

Figure 31 Ionospheric response to the precipitation events during the 0900 to 1100 UT period on 16 February, 1980. Peak electron density and altitude of ionization maximum are plotted vs. time.

total energy deposit and mean energy parameter observed in the spectrophotometric emissions. If the spectrophotometric data are interpreted in terms of the altitude of maximum auroral emission, a comparison between radar and optical aspects of the auroral phenomena over the experimentl period may be made. Figure 32 illustrates the slow decay in precipitation and excitation intensity over the 2 1/2 hour experimental period which is exhibited as the slow rise in the altitude computed for the peak emission intensity. The qualitative covariance between these independent measurements appears to be very good. The spectrophotometric data, at late times shows a higher altitude for peak emission, however this feature is probably caused by residual emission of 630. nm intensity from the F-region as well as by transport of ionization and excited states at the higher altitudes.

3.5 Overall Results of Coordinated Experiments

Measurements of the characteristics of auroral spectrophotometric emissions and of the ionospheric electron density vs. altitude have allowed detailed comparitive measurements of the precipitating electron flux parameters as well as the ionospheric response to the auroral disturbance. These coordinated measurements provide cross-calibrated results over a wide range of auroral precipitation conditions, and will allow application of both radar and spectrophotometric measurements to the construction and verification of predictive models for nuclear and natural interference to both optical and electromagnetic propagation systems.

The coordinated measurements and their results may be summarized as follows:

- Spectrophotometric measurements of intense transient precipitation events may be interpreted in terms of the ionospheric electron density perturbations as well as the visible and IR optical excitation characteristics. In the case of the time-dependent variations of electron density, the recombination relaxation time must be taken into account.
- The range of cross-calibration between radar- and optically-derived quantities descriptive of the precipitating particle flux

and the response of the auroral ionosphere has been extended to auroral conditions involving intense transient events and to the opposite extreme of very soft, moderately energetic precipitation events.

- The results of the coordinated experiments show that much useful information on energetic particle precipitation, excitation of visible, near IR, and IR active species, and the response of the ionospheric electron density to natural and artificial perturbations may be derived from spectrophotometric observations alone.
- On the basis of the results cited above, spectrophotometric support of future DNA/AFGL experiments should provide valuable data.

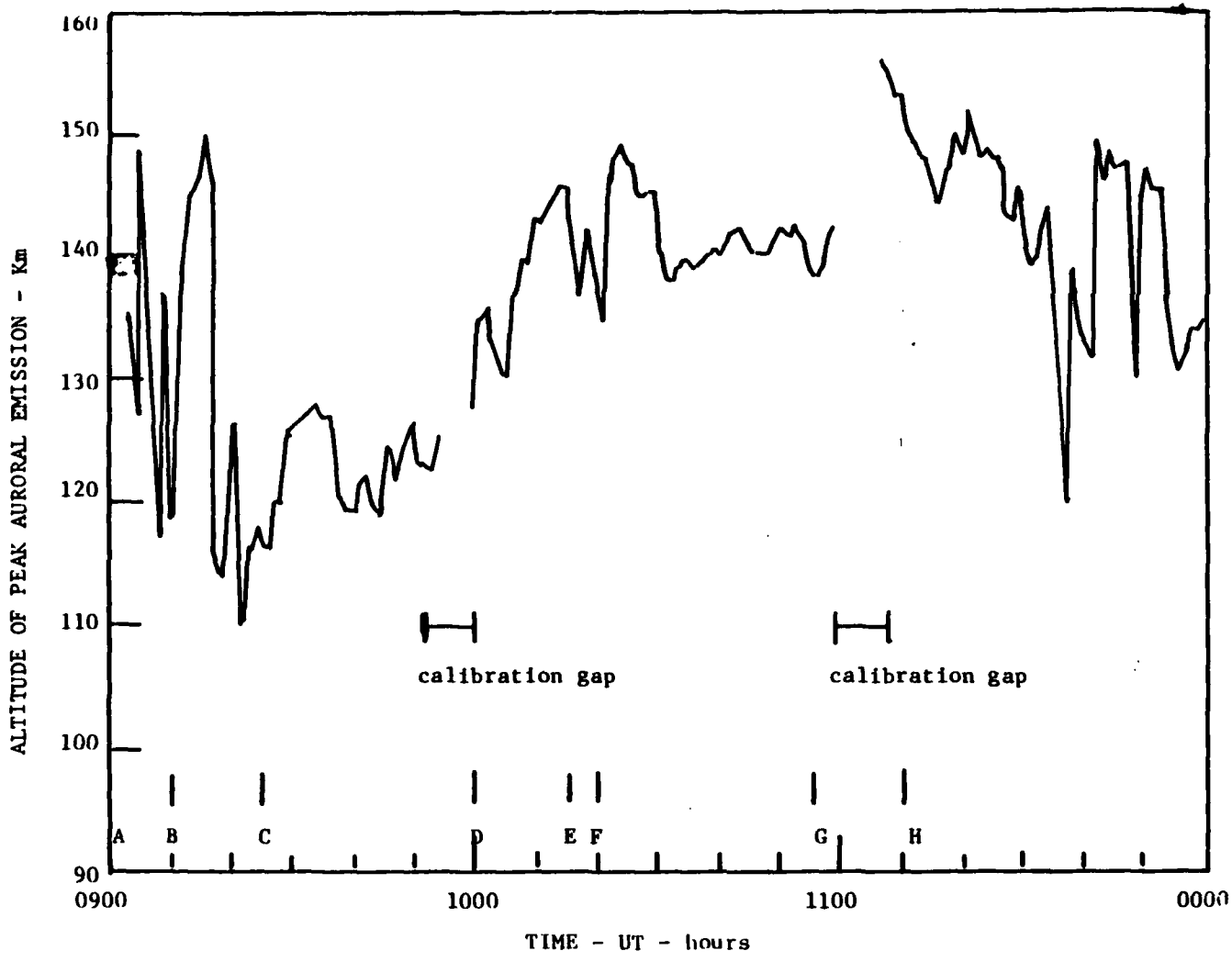

Figure 32 Altitude of the peak optical emission vs. time as derived from spectrophotometric data. The slow increase in altitude over the time period is a consequence of the slowly decreasing mean energy parameter of the precipitating electrons.

4. CONCLUSIONS AND RECOMMENDATIONS

4.1 Conclusions

Improvements to the spectrophotometric instrumentation and the analytical software have allowed more definitive measurements of the structure of auroral emissions to be made. From these structure measurements, improved computations of temporal and spatial PSD's provide a useful data base for development and evaluation of predictive models of IR radiance intensity and structure in bands of interest to systems operations.

Coordinated spectrophotometric experiments conducted at Chatanika, Alaska in cooperation with the SRI Internation incoherent scatter radar facility have extended the useful range of cross-calibrated quantities, ie., those quantities relevant to the precipitating electron flux, its excitation of optically active species vs. time and altitude, and the response of the ionosphere to the particle flux. The cross calibration effort has shown that in many cases, spectrophotometric data may be utilized to provide a relatively complete picture of the aurora input phenomenology as well as a description of some of its output effectsin both optical radiance and ionization regimes. As such, spectrophotometric data will become more important for support of future DNA/AFGL rocket experiments in Alaska after the incoherent radar is moved.

Reference to Table 3, section 1 indicates the degree to which the cross calibration and verification of spectrophotometric measurements has been extended for interpretation in terms of optical and ionospheric parameters which provide input to systems disturbance models.

4.2 Recommendations

The present spectrophotometric instrument complement and the supporting data acquisition, data reduction and analysis software are currently capable of providing significant ground-based optical support to future DNA/AFGL experiments. However, to satisfy present and future systems related data requirements, several hardware and software improvement initiatives are recommended. These are:

- o Improve the sensitivity and spatial resolution of present instrumentation for measurement of auroral and airglow spatial structure, especially in the near IR bands of OH and $O_2(^1\ )$.
- o Develop a dedicated DNA/AFGL spectrally selective imaging system using image intensified TV (IITV) or solid state detector arrays to cover both visible and near IR spectral ranges. Such a system is critical to furthur support of experiments such as ELIAS, CIRRUS, SPIRIT, and other systems related experiments. At present, the IITV system compatible with the BRIM analysis requirements is available only on a non-interference loan basis, and may not be optimized to satisfy DNA/AFGL requirements for future measurements.
- o A long range support plan should be developed such that the proper ground-based spectrophotometric instrumentation can be prepared and made available to forthcoming DNA/AFGL experiments on a timely basis.
- o Furthur analyses of OH structure data should be undertaken. Data available to date has a relatively low signal to noise ratio, hence requires more careful handling than resources available at present have allowed. A specific program relating to derivation of OH emission temporal and spatial PSD's and their applications to systems should be initiated, based upon the present data base. This effort then would provide guidance for future measurements of OH radiance structure and would assist in formulating an OH structure data base for systems effects modeling.

5. REFERENCES

1. Sears, R. D., Coordinated Measurements of Ionospheric Irregularities: Digital Photometer Design and Development, Topical Report, Contract DASA 01-71-C-0158, LMSC D311213, 20 October, 1972.
2. Sears, R. D., Definition of Energy Input: Operation ICE CAP, Final Report, Contract DNA 01-72-C-0134, DNA 2985F, LMSC D311131, 1 Oct. 1972.
3. Sears, R. D., Ionospheric Irregularities: Alaska Photometric Measurements, Final Report, Contract DNA 001-73-C-0110, DNA 3235F, 4 December, 1973.
4. Sears, R. D., J. E. Evans, and R. N. Varney, ICE CAP Analysis: Mechanisms for Energy Deposit in the Auroral Ionosphere, Final Report, Contract DNA 001-73-C-0224, DNA 3293F, 15 January, 1974.
5. Sears, R. D., Ionospheric Irregularities: Auroral Motions and Plasma Drifts, Final Report, Contract DNA 001-74-C-0179, DNA 3514, LMSC D405729, 30 September, 1974.
6. Sears, R. D., ICE CAP Analysis: Energy Deposit and Transport in the Auroral Ionosphere, ICE CAP 73-74, Final Report, Contract DNA 001-73-C-0224, DNA 3566F, 15 November, 1974.
7. Sears, R. D., "Versatile Family of Modular Aurora and Airglow Photometers," Appl. Optics, Vol. 12, pp. 1349-1355, 1973.
8. Sears, R. D., "Intensity Correlations of the 4278A N_2^+ (0-1) First Negative Band and 5875A Emissions in Auroras," J. Geophys. Res, Vol 80, pp. 215-217, 1975.
9. Sears, R. D., and J. E. Evans,"Coordinated Optical and Radar Measurements of Auroral Motions and Ionos-heric Plasma Drift," Atmospheres of the Earth and Planets, Ed. B. M. McCormac, D. Reidel Pub. Co. , 1974.
10. Sears, R. D., Ionospheric Irregularities, HAES Program Support, Final Report, Contract DNA 001-75-C-0098, 30 September, 1975.
11. Sears, R. D., Ionospheric Irregularities: Optical Support of HAES Scintillation Experiments, Final Report, Contract DNA 001-76-C-0182, DNA 4240F, 31 January 1977.

12. Sears, R. D., Ground-Based Photometric Measurements: HAES Program Support, Technical Report, Contract DNA 001-77-C-0329, 31 January, 1979, DNA 4975Z.

13. Kumer, J., Furthur Evaluation of ICE CAP Auroral 4.3 um Zenith Radiance, Final Report, Contract DNA 001-76-C-0015, 1976.

14. Leadabrand, R. L., M. J. Baron, J. Petriceks, and H. G. Bates, "Chatanika Alaska Auroral Zone Incoherent Scatter Facility," Radio Science Vol. 7, 747-756, 1972.

15. Vondrak, R. R., and M. J. Baron, "Radar Measurements of the Latitudinal Variation of Auroral Ionization," Radio Science, Vol. 11, pp. 939-946, 1976.

16. Vondrak, R. R., and M.J. Baron, "A Method of Obtaining the Energy Distribution of Auroral Electrons from Incoherent Scatter Radar Measurements," Radar Probing of the Auroral Plasma, Proceedings of the EISCAT Summer School, Tromso, Norway, June 5-13, 1975. A. Brekke (Ed.) pp. 315-330, Universitetsforlaget, Tromso-Oslo-Bergen, 1977.

17. Chamberlain, J., Physics of the Aurora and Airglow, Academic Press, New York, 1961.

18. Vallance Jones, A., Aurora, D. Reidel Pub. Co., Dordrecht Holland, 1974.

19. Eather, R. H., "Radiation from Positive Particles Penetrating the Auroral Atmosphere," J. Geophys. Res., Vol. 71, 4133, 1966.

20. Rees, M. H., and D. Luckey, "Auroral Electron Energy Derived from the Ratio of Spectroscopic Emissions: 1. Model Computations," J. Geophys. Res., Vol. 79, 5181-5186, 1974.

21. Wickwar, V. B., M. J. Baron, and R. D. Sears, "Auroral Energy Input from Energetic Electrons and Joule Heating at Chatanika," J. Geophys. Res., Vol. 80, 4364, 1975.

22. Vondrak, R. R., "Remote Sensing of High Latitude Ionization Profiles by Ground-based and Spaceborne Instruments," Symposium on the Effects of the Ionosphere on Radiowave Systems, Alexandria, Va., 1981.

23. Burger, M. J., S. M. Seltzer, and K. Maeda, "Energy Deposition by Auroral Electrons in the Atmosphere," J. Atmos. Terr. Phys, Vol 36, pp. 1015-1045, 1970.

24. Rees, M. H., "Auroral Ionization and Excitation by Incident Energetic Electrons," Planet. Space Sci., Vol. 11, pp. 1209-1218, 1963.

25. Walt, M., W. M. MacDonald, and W. E. Francis, "Penetration of Auroral Electrons in the Atmosphere," Physics of the Magnetosphere, R. L. Carovillano and J. F. McClay, eds., p 534, Reinhold Book Co. New York, N.Y., 1968.

26. Vondrak, R. R., and R. D. Sears, "Comparison of Incoherent Scatter Radar and Photometric Measurements of the Energy Distribution of Auroral Electrons," J. Geophys. Res., Vol. 83, pp. 1665-1667, 1978.

27. Sears, R. D., and R. R. Vondrak, "Optical Emissions and Ionization Profiles During an Intense Pulsating Aurora, "J. Geophys. Res., Vol. 86 pp. 6853-6858, 1981.

28. Davidson, G., and R. D. Sears, "Pulsating Auroras: Evidence for Flux Limiting, "Geophys. Res. Letters, Vol. 7, 185, 1980.

APPENDIX A

DATA SYNOPSIS SHEETS

SYNOPSIS OF DATA

Tape: AGIN 10

Date: 29 January, 1979 **Time:** 0530-1400 UT

Photometer(s): 3B1, 3C

General Activity:

0600-1000 UT	Clear Sky, no activity
1000-1120 UT	Weak arcs to north
1120-1230 UT	Westward surge in north, breakup with negative bay
1230-1350 UT	Weak, erratic pulsating patches

Operating Modes:

0640-1350 UT	3B1 on 4278A
0640-1300 UT	3C on scan mode, 10- 170 degrees, 4 degree interval 2 second dwell time each angle *
1300-1350 UT	3C on magnetic zenith, coordination with radar

Notes:

* This scan mode is the standard mode of operation for meridional scans. All subsequent data sheets using this mode will identify it by "standard mode".

During this operating period, the digital clock was stuck at 070xxx.

SYNOPSIS OF DATA

Tape: AGIN 11

Date: 2 February, 1979 **Time:** 0345 - 1200 UT

Photometer(s): 3B1, MTP, 3C

General Activity:

0500-0700 UT Auroral activity to north, thin clouds to zenith, moon up
0700-0800 UT Activity to zenith, sky clear
0800-0830 UT Faint Pulsat ng patches
0910-1140 UT* Faint pulsating patches

Operating Modes:

0540-1120 UT , 3B1 and MTP on OH bands
1120-1140 UT , 3B1 and MTP on 4278A
0540-1120 UT, 3C, Standard scan mode
1120-1140 UT, 3C, Magnetic Zenith for radar coordination

Notes:

* Several successive power failures precluded data acquisition between about 0830 and 0910 UT.

SYNOPSIS OF DATA

Tape: AGIN 12

Date: 3 February 1979 **Time:** 0630-1200 UT

Photometer(s): 3B1, MTP, 3C

General Activity:

0800- 1150 UT No activity, clear sky, moon up in early evening

Operating Modes:

0800-1150 3c , Standard scan mode, 3B1 and MTP on OH bands

Notes:

SYNOPSIS OF DATA

Tape: AGIN 13

Date: 5 February, 1979 **Time:** 0450-1330 UT

Photometer(s): 3B1, MTP, 3C

General Activity:

0530-0600 UT Arc visible to north, moon up
0600-0900 UT No activity, moon up
0900-1230 UT Variable activity, arc moves to S of zenith, poleward expansion diffuse aurora over sky

Operating Modes:

0500-0920 UT 3B1 and MTP on OH bands
0920-1300 UT 3B1 and MTP on 4278A
0500-1300 UT 3C on standard scan mode

Notes:

SYNOPSIS OF DATA

Tape: AGIN 14

Date: 6 February 1979 **Time:** 0655-1300 UT

Photometer(s): 3B1, MTP, 3C

General Activity:

0700-0945 UT	No activity
0945-1245 UT	Active, arcs to north, breakup, activity over sky, then multiple bands to north

Operating Modes:

0705-1245 UT 3B1, MTP on OH Bands, 3C on Standard scan mode

Notes:

SYNOPSIS OF DATA

Tape: PULSE 01

Date: 11 February 1980 **Time:** 0700-0925 UT

Photometer(s): 3B1, 3C

General Activity:

0740-0820 UT No activity

0820 - Clouded up

Operating Modes:

0720-0840 3B1, 4278A; 3C Standard scan mode

Notes:

SYNOPSIS OF DATA

Tape: PULSE 02

Date: 14 February 1980 **Time:** 0400-1310 UT

Photometer(s): 3B1, 3C

General Activity:

0400-0800 UT Quiet, clear sky

0800 - 1200 UT Acitivity increased to entire sky with some small pulsations

Operating Modes:

0430- 0930 UT, 3B1 on 4278A; 3C standard scan mode

0930-1300 UT, 3C at magnetic zenith

0930-1045 UT, 3B1 on 4278, then shut down

Notes:

Coordinated magnetic zenith runs with Chatanika radar from 0930 to 1300 UT.

SYNOPSIS OF DATA

Tape: PULSE 03

Date: 15 February 1980 **Time:** 0505 - 1045 UT

Photometer(s): 3B1, 3C

General Activity:

0535-0700 UT No activity

0700-1010 UT Activity increases, arcs and bands to zenith

Operating Modes:

0535-1010 UT 3C, standard scan mode

Notes:

Work was being done on 3B1 during this observing period: no useful data.

SYNOPSIS OF DATA

Tape: PULSE 04

Date: 16 February 1980 **Time:** 0440 - 1300 UT

Photometer(s): 3B1, 3C

General Activity:

0500-1250 UT Very active throughout observing period

0925 and after Intense pulsating patches at magnetic zenith

Operating Modes:

0500-0900 UT 3C, standard scan mode; 3B1,4278A
0900-1250 UT 3C, at magnetic zenith, 3B1 , 4278A

Notes:

During part of this observing period, strong sunward forms were observed extending from the main substorm which was far to the south. Data from 0900 to 1250 UT coordinated with radar measurements at magnetic zenith.

SYNOPSIS OF DATA

Tape: PULSE 05

Date: 17 February 1980 **Time:** 0500-0840 UT

Photometer(s): 3B1, 3C

General Activity:

0530-0830 No activity

0830 and after, increasing haze.

Operating Modes:

0530-0830 UT 3B1, 4278A; 3C, standard scan mode

Notes:

SYNOPSIS OF DATA

Tape: PULSE 06

Date: 18 February 1980 **Time:** 1520-1225 UT

Photometer(s): 3B1, 3C

General Activity:

0540-0700 UT Quiet

0700-1245 UT Arcs come up from north, moderate intensity, diffuse aurora no noticeable breakup or magnetic activity

Operating Modes:

0540-0730 UT 3C, standard scan mode; 3B1 on OH bands

0730-1245 UT 3C, as before, 3B1 on 4278A.

Notes:

DISTRIBUTION LIST

DEPARTMENT OF DEFENSE

Defense Nuclear Agency
ATTN: RAAE, P. Lunn
ATTN: RAEE
3 cy ATTN: RAAE
4 cy ATTN: TITL

Defense Technical Info Center
12 cy ATTN: DD

Field Command
DNA/Det 1
Lawrence Livermore Lab
ATTN: FC-1

DEPARTMENT OF THE ARMY

BMD Advanced Technology Center
ATTN: ATC-T, M. Capps
ATTN: ATC-O, W. Davies
ATTN: ATC-R, W. Dickinson
ATTN: ATC-R, D. Russ

BMD Systems Command
2 cy ATTN: BMDSC-HW

US Army Satellite Comm Agency
ATTN: Document Control

US Army Tradoc Sys Analysis Actvy
ATTN: ATAA-TDC
ATTN: ATAA-PL
ATTN: ATAA-TCC, F. Payan Jr

DEPARTMENT OF THE NAVY

Naval Research Laboratory
ATTN: Code 4780, S. Ossakow
ATTN: Code 6700
ATTN: Code 7950, J. Goodman

Office of Naval Research
ATTN: Code 412, W. Condell
ATTN: Code 414, G. Joiner

DEPARTMENT OF THE AIR FORCE

Air Force Geophysics Laboratory
ATTN: OPR, H. Gardiner
ATTN: OPR-1
ATTN: LKB, K. Champion
ATTN: CA, A. Stair
ATTN: R. O'Neil
ATTN: PHP
ATTN: PHI, J. Euchau
ATTN: R. Babcock

Air Force Technical Applications Ctr
ATTN: TN

Space Division
ATTN: YGJB, W. Mercer

Space Division
ATTN: YKM, Maj Alexander
ATTN: YKM, Capt Norton

OTHER GOVERNMENT AGENCIES

Institute for Telecommunications Sciences
ATTN: A. Jean
ATTN: W. Utlaut
ATTN: L. Berry

DEPARTMENT OF ENERGY CONTRACTORS

EG&G, Inc
ATTN: J. Colvin
ATTN: D. Wright

University of California
Lawrence Livermore National Lab
ATTN: L-31, R. Hager
ATTN: L-389, R. Ott
ATTN: Technical Info Dept Library

Los Alamos National Laboratory
ATTN: P. Keaton
ATTN: C. Westervelt
ATTN: R. Jeffries
ATTN: T. Kunkle, ESS-5
ATTN: D. Simons
ATTN: MS 664, J. Zinn
ATTN: MS 670, J. Hopkins
ATTN: J. Wolcott

Sandia National Labs, Livermore
ATTN: T. Cook
ATTN: B. Murphy

DEPARTMENT OF DEFENSE CONTRACTORS

Aerospace Corp
ATTN: I. Garfunkel
ATTN: D. Olsen
ATTN: J. Straus
ATTN: V. Josephson
ATTN: T. Salmi
ATTN: R. Slaughter

Berkeley Research Associates, Inc
ATTN: J. Workman
ATTN: S. Brecht
ATTN: C. Prettie

Cornell University
ATTN: M. Kelly
ATTN: D. Farley Jr

HSS, Inc
ATTN: D. Hansen

Kaman Tempo
ATTN: DASIAC

Lockheed Missiles & Space Co, Inc
ATTN: J. Kumer
4 cy ATTN: R. Sears

Pacific-Sierra Research Corp
ATTN: H. Brode, Chairman SAGE

Photometrics, Inc
ATTN: I. Kofsky

DEPARTMENT OF DEFENSE CONTRACTORS (Continued)

Lockheed Missiles & Space Co, Inc
ATTN: C. Old, Dept 6821
ATTN: D. Churchill, Dept 81-11
ATTN: Dept 60-12

Mission Research Corp
ATTN: R. Hendrick
ATTN: Tech Library

R&D Associates
ATTN: W. Wright
ATTN: F. Gilmore
ATTN: R. Turco
ATTN: M. Gantsweg

SRI International
ATTN: W. Chesnut
ATTN: M. Baron
ATTN: C. Rino

DEPARTMENT OF DEFENSE CONTRACTORS (Continued)

Science Applications, Inc
ATTN: D. Hamlin

Stewart Radiance Laboratory
ATTN: J. Ulwich

Technology International Corp
ATTN: W. Boquist

Utah State University
ATTN: Sec Con Ofc for D. Burt
ATTN: Sec Con Ofc for K, Baker, Dir Atmos & Space Sci
ATTN: Sec Con Ofc for A. Steed

Visidyne, Inc
ATTN: J. Carpenter
ATTN: C. Humphrey
ATTN: W. Reidy